MATCH
Communications in Mathematical and in Computer Chemistry

MATCH Commun. Math. Comput. Chem. **55** (2006) 237-270

ISSN 0340 - 6253

Combinatorial Enumeration of Stereoisomers by Linking Orbits in Molecules with Orbits Among Molecules. A Novel Way of Stereochemistry Through the Concepts of Coset Representations and Sphericities (Part 3)

Shinsaku Fujita
Department of Chemistry and Materials Technology,
Kyoto Institute of Technology,
Matsugasaki, Sakyoku, Kyoto 606-8585, Japan
E-mail: fujitas@chem.kit.ac.jp

(Received: May 16, 2005)

Abstract

The present series is devoted to a diagrammatical introduction to the USCI (unit-subduced-cycle-index) approach developed by Fujita (S. Fujita, "Symmetry and Combinatorial Enumeration in Chemistry", Springer-Verlag, 1991). In Part 3 of this series, intramolecular stereochemistry (Part 1) and intermolecular stereochemistry (Part 2) are integrated in terms of *reduced mandalas* so as to provide versatile tools for enumerating stereoisomers, i.e., the SCI (subduced-cycle-index) method and the PCI (partial-cycle-index) method. The methodology which these methods depend upon is diagrammatically demonstrated, where two modes of views (i.e., "column view" and "row view") are applied to the mark table of $\mathbf{D}_{2d}$ in stereoisomer enumeration based on an allene skeleton of $\mathbf{D}_{2d}$-symmetry.

1 Introduction

Chemical combinatorics has been one of the central themes in the application of mathematics to chemistry [1]. Although Pólya's theorem has widely applied to combinatorial enumeration of groups, graphs, and chemical compounds [2, 3], it has been shown in recent papers [4, 5] that the chemical compounds enumerated by Pólya's theorem are "graphs", but not "stereoisomers" (three-dimensional objects). Moreover, Pólya's theorem is incapable of itemizing chemical compounds (enumerated as graphs) with respect to point-group symmetries. The enumeration of stereoisomers has been successfully accomplished by Fujita's USCI (unit-subduced-cycle-index) approach [6], where the evaluated numbers of stereoisomers are itemized with respect to molecular formulas as well as to point-group symmetries. The enumeration of stereoisomers has required the development of new concepts, i.e., *subductions of coset representations* and *sphericities*. Although a mathematical treatment of how these concepts are applied to chemical combinatorics has been described in Chapters 13–19 of Fujita's book [6], it is desirable to provide an educational version that consists of diagrammatical explanation and illustrative examples.

In Part 1 of this series [7] for a diagrammatical introduction of Fujita's USCI (unit-subduced-cycle-index) approach [6], the concepts of *coset representations* and *sphericities* have been shown to work well in intramolecular stereochemistry, where these concepts have been explained diagrammatically by starting from the concept of *regular bodies*. In Part 2 of this series [8], the concepts of *coset representations* and *sphericities* have been demonstrated to work also in intermolecular stereochemistry (stereoisomerism), where they have been explained diagrammatically by starting from the concepts of *mandalas* and *reduced mandalas* defined as nested regular bodies. As Part 3 of this series, the present article is intended to provide a foundation of chemical combinatorics by integrating Part 1 and Part 2, where *the subductions of coset representations* applied concurrently to regular bodies and (reduced) mandalas will be shown to be a key concept for linking the intramolecular stereochemistry and the intermolecular one.

2 Fixed-Point Vectors as Ordered Sets of Marks

In continuation of Parts 1 and 2, allene derivatives belonging to the point group $\mathbf{D}_{2d}$ and its subgroups are used as examples. According to Part 1, a non-redundant set of subgroups (SSG) for $\mathbf{D}_{2d}$ is selected as follows:

$$\mathrm{SSG}_{\mathbf{D}_{2d}} = \{\mathbf{C}_1, \mathbf{C}_2, \mathbf{C}'_2, \mathbf{C}_s, \mathbf{S}_4, \mathbf{C}_{2v}, \mathbf{D}, \mathbf{D}_{2d}\}, \tag{1}$$

where a representative is selected from each set of conjugate subgroups; and the subgroups are aligned in an ascending order of their orders ($|\mathbf{C}_1| = 1$, $|\mathbf{C}_2| = 2$, $|\mathbf{C}'_2| = 2$, $|\mathbf{C}_s| = 2$, $|\mathbf{S}_4| = 4$, $|\mathbf{C}_{2v}| = 4$, $|\mathbf{D}| = 4$, and $|\mathbf{D}_{2d}| = 8$). The subgroups of $\mathbf{D}_{2d}$ are categorized into two types: chiral subgroups ($\mathbf{D}$, $\mathbf{C}_2$ $\mathbf{C}'_2$, and $\mathbf{C}_1$) that consist of proper rotations only and achiral subgroup ($\mathbf{D}_{2d}$, $\mathbf{C}_{2v}$, $\mathbf{S}_4$, $\mathbf{C}_s$) that consist of proper and improper rotations.

2.1 Reduced Mandalas and Fixed-Point Vectors

As shown in Part 2 for the case of $\mathbf{G} = \mathbf{D}_{2d}$, an $\mathbf{H}$-molecule ($\mathbf{H} \subset \mathbf{G}$), which is derived from a $\mathbf{G}$-skeleton with a $\mathbf{G}(/\mathbf{H}')$-orbit (e.g., $\mathbf{H}' \subset \mathbf{G}$) of substitution positions, generates an orbit of $\mathbf{H}$-assemblies in a reduced mandala, where the orbit is governed by a CR $\mathbf{G}(/\mathbf{H})$. The CR is

Table 1: USCI-CFs and Marks for $\mathbf{D}_{2d}$ [6]

USCI-CFs for Positions of a $\mathbf{D}_{2d}$-Skeleton

$\mathbf{D}_{2d}(/\mathbf{C}_1)$	b_1^8	b_2^4	b_2^4	c_2^4	c_4^2	c_4^2	b_4^2	c_8
$\mathbf{D}_{2d}(/\mathbf{C}_s)$	b_1^4	b_2^2	b_2^2	$a_1^2c_2$	c_4	a_2^2	b_4	a_4
	$\updownarrow$	$\updownarrow$	$\updownarrow$	$\updownarrow$	$\updownarrow$	$\updownarrow$	$\updownarrow$	$\updownarrow$

Marks for a Reduced Mandala of $\mathbf{D}_{2d}$-Symmetry

	$\downarrow\mathbf{C}_1$	$\downarrow\mathbf{C}_2$	$\downarrow\mathbf{C}_2'$	$\downarrow\mathbf{C}_s$	$\downarrow\mathbf{S}_4$	$\downarrow\mathbf{C}_{2v}$	$\downarrow\mathbf{D}_2$	$\downarrow\mathbf{D}_{2d}$
$\mathbf{D}_{2d}(/\mathbf{C}_1)$	8	0	0	0	0	0	0	0
$\mathbf{D}_{2d}(/\mathbf{C}_2)$	4	4	0	0	0	0	0	0
$\mathbf{D}_{2d}(/\mathbf{C}_2')$	4	0	2	0	0	0	0	0
$\mathbf{D}_{2d}(/\mathbf{C}_s)$	4	0	0	2	0	0	0	0
$\mathbf{D}_{2d}(/\mathbf{S}_4)$	2	2	0	0	2	0	0	0
$\mathbf{D}_{2d}(/\mathbf{C}_{2v})$	2	2	0	2	0	2	0	0
$\mathbf{D}_{2d}(/\mathbf{D}_2)$	2	2	2	0	0	0	2	0
$\mathbf{D}_{2d}(/\mathbf{D}_{2d})$	1	1	1	1	1	1	1	1

characterized by the $\mathbf{G}(/\mathbf{H})$-row of the mark table. Note that the CR $\mathbf{G}(/\mathbf{H}')$ is concerned with intramolecular stereochemistry (cf. Part 1), while the CR $\mathbf{G}(/\mathbf{H})$ is concerned with intermolecular stereochemistry (cf. Part 2), where the global symmetry $\mathbf{G}$ is commonly effective and the local symmetry $\mathbf{H}$ in the CR $\mathbf{G}(/\mathbf{H})$ causes the subduction $\mathbf{G}(/\mathbf{H}') \downarrow \mathbf{H}$.

The CR $\mathbf{G}(/\mathbf{H})$ corresponding to an $\mathbf{H}$-molecule (via an $\mathbf{H}$-assembly) is subduced into a subgroup $\mathbf{K}$ in order to obtain the mark (the number of fixed points) for the subduction $\mathbf{G}(/\mathbf{H}) \downarrow \mathbf{K}$. When $\mathbf{K}$ runs over the SSG (e.g., eq. 1 for $\mathbf{D}_{2d}$), the resulting marks construct a fixed-point vector (FPV) for the CR $\mathbf{G}(/\mathbf{H})$. Such FPVs appear as $\mathbf{G}(/\mathbf{H})$-rows of the mark table of $\mathbf{G}$, as exemplified by Table 1 for $\mathbf{D}_{2d}$.[1]

In Fujita's USCI approach, the CR $\mathbf{G}(/\mathbf{H})$ for stereoisomerism is characterized by the marks corresponding to the subductions $\mathbf{G}(/\mathbf{H}) \downarrow \mathbf{K}$ where $\mathbf{K}$ is varied. In other words, the $\mathbf{G}(/\mathbf{H})$-row of the mark table (e.g., Table 1 for $\mathbf{D}_{2d}$) is used for the characterization of an $\mathbf{H}$-molecule. On the other hand, the CR $\mathbf{G}(/\mathbf{H}')$ for intramolecular stereochemistry is characterized by the USCI-CFs corresponding to $\mathbf{G}(/\mathbf{H}') \downarrow \mathbf{K}$, as shown in the top of Table 1 in the case of $\mathbf{G} = \mathbf{D}_{2d}$.

In order to discuss the properties of mark tables according to the present context, Proposition 180 described in Chapter 12 of Burnside's book [9] is restated as the following theorem:[2]

Theorem 1. *The mark (the number of fixed points) for* $\mathbf{G}(/\mathbf{H}) \downarrow \mathbf{K}$ *is a non-zero integer if* $\mathbf{K} \subset \mathbf{H}$. *Otherwise, the mark for* $\mathbf{G}(/\mathbf{H}) \downarrow \mathbf{K}$ *is equal to zero. Note that the subgroup* $\mathbf{H}$ *(or* $\mathbf{K}$*) and its conjugates are equalized under the group* $\mathbf{G}$.

Theorem 1 provides us with the reason for why each mark table is regarded as a lower triangular matrix [9]. According to Theorem 1, mark tables such as Table 1 can be interpreted

[1] Although this table is essentially the same as Table 11 of Part 1, some additional data are combined with the original form reported in Part 1.

[2] Coset representations described in the present series and in Fujita's book [6] are equivalent to transitive permutation groups described in Burnside's book [9].

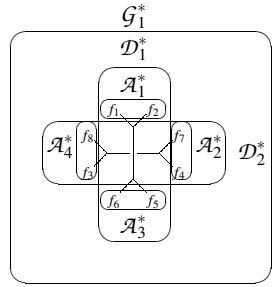

Figure 1: Subgroup-supergroup relationships of $\mathbf{C}_s$-, $\mathbf{C}_{2v}$-, and $\mathbf{D}_{2d}$-assemblies in a reduced mandala of $\mathbf{D}_{2d}$-symmetry. They determine the marks appearing in the $\downarrow \mathbf{C}_s$-column of the mark table of $\mathbf{D}_{2d}$, where the resulting marks correspond to the CR $\mathbf{D}_{2d}(/\mathbf{C}_s)$ for the orbit of $\mathbf{C}_s$-assemblies (i.e., $\mathcal{A}^* = \{\mathcal{A}_1^*, \mathcal{A}_2^*, \mathcal{A}_3^*, \mathcal{A}_4^*\}$), to the CR $\mathbf{D}_{2d}(/\mathbf{C}_{2v})$ for the orbit of $\mathbf{C}_{2v}$-assemblies (i.e., $\mathcal{D}^* = \{\mathcal{D}_1^*, \mathcal{D}_2^*\}$), and to the CR $\mathbf{D}_{2d}(/\mathbf{D}_d)$ for the orbit of a $\mathbf{D}_{2d}$-assembly (i.e., $\mathcal{G}^* = \{\mathcal{G}_1^*\}$).

in two ways:

1. **Row view**: Suppose that the **H** in the CR **G**(/**H**) is fixed for the sake of convenience. When **K** of the subduction $\mathbf{G}(/\mathbf{H}) \downarrow \mathbf{K}$ runs over the SSG of **G**, the resulting marks give the FPV corresponding to the CR $\mathbf{G}(/\mathbf{H})$, i.e., the $\mathbf{G}(/\mathbf{H})$-row of the mark table.

2. **Column view**: On the other hand, when **L** of the subduction $\mathbf{G}(/\mathbf{L}) \downarrow \mathbf{H}$ runs over the SSG of **G**, the resulting marks appear in the $\downarrow \mathbf{H}$-column of the mark table, where **H** is fixed.

Although Theorem 1 is written by a mathematical expression, its meaning can be diagrammatically explained by using reduced mandalas. In particular, the second item (the column view) is important to evaluate the marks of the $\downarrow \mathbf{H}$-column. For example, Fig. 1 shows the subgroup-supergroup relationship for evaluating marks for the $\downarrow \mathbf{C}_s$-column by using assembled reduced mandalas. As found easily, the $\mathbf{C}_s$-assemblies ($\mathcal{A}^* = \{\mathcal{A}_1^*, \mathcal{A}_2^*, \mathcal{A}_3^*, \mathcal{A}_4^*\}$) are contained in the $\mathbf{C}_{2v}$-assemblies ($\mathcal{D}^* = \{\mathcal{D}_1^*, \mathcal{D}_2^*\}$), which are, in turn, contained in the $\mathbf{D}_{2d}$-assemblies ($\mathcal{G}^* = \{\mathcal{G}_1^*\}$). The $\downarrow \mathbf{C}_s$-operation on the reduced mandala with such multiple assemblage (Fig. 1) fixes one or more assemblies so that the subductions, $\mathbf{D}_{2d}(/\mathbf{C}_s) \downarrow \mathbf{C}_s$, $\mathbf{D}_{2d}(/\mathbf{C}_{2v}) \downarrow \mathbf{C}_s$, and $\mathbf{D}_{2d}(/\mathbf{D}_{2d}) \downarrow \mathbf{C}_s$, give marks of non-zero integers, as assured by Theorem 1. When **L** for $\mathbf{D}_{2d}(/\mathbf{L}) \downarrow \mathbf{C}_s$ is not a supergroup of $\mathbf{C}_s$, each of **L**-assemblies is not fixed by $\mathbf{C}_s$ so that the corresponding marks are equal to zero ($\mathbf{L} = \mathbf{C}_1, \mathbf{C}_2, \mathbf{C}_2'$ for $|\mathbf{L}| \leq |\mathbf{C}_s|$; and $\mathbf{L} = \mathbf{S}_4, \mathbf{D}_2$ for $|\mathbf{L}| > |\mathbf{C}_s|$).

Because the case of $\mathbf{L} = \mathbf{H}$ is the threshold of zero/non-zero values for Theorem 1, the subduction $\mathbf{G}(/\mathbf{H}) \downarrow \mathbf{H}$ is informative to discuss the marks in the FPV for the CR $\mathbf{G}(/\mathbf{H})$. Then, the subduction $\mathbf{G}(/\mathbf{L}) \downarrow \mathbf{H}$ for $\mathbf{L} \supset \mathbf{H}$ is examined to evaluate the marks of the $\downarrow \mathbf{H}$-column. This task is the subject of the next subsection.

2.2 Row View and Column View for Evaluation of FPVs

Although the terms "row view" and "column view" have not explicitly been used in Fujita's USCI approach, Chapter 15 (Section 15.2) of Fujita's book [6] has discussed each column of a fixed-point matrix (FPM). This treatment is essentially based on the same methodology as the present "column view". The present terms "row view" and "column view", however, have a more diagrammatical basis through the concepts of mandalas and reduced mandalas.

2.2.1 $\mathbf{D}_{2d}$-Molecules

Row View for $\mathbf{D}_{2d}$-Molecules. Let us consider allene as a $\mathbf{D}_{2d}$-skeleton, the substitution positions of which are governed by the CR $\mathbf{D}_{2d}(/\mathbf{C}_s)$, where we place $\mathbf{G} = \mathbf{D}_{2d}$ and $\mathbf{H}' = \mathbf{C}_s$. By numbering the four positions sequentially, allene itself is considered to be generated by a function f, where we place $f(1) = \mathrm{H}$, $f(2) = \mathrm{H}$, $f(3) = \mathrm{H}$, and $f(4) = \mathrm{H}$ (Fig. 2). Because the resulting transformula (**2**) belongs to $\mathbf{D}_{2d}$, the action of the symmetry operations of $\mathbf{D}_{2d}$ transforms **2** (f_1) into the transformulas (**2**–**9**, i.e., f_1–f_8),[3] which are identical with one another without taking the numbering of vertices (substitution positions) into consideration. Thereby, the reduced mandala shown in Fig. 2 is obtained so as to show the symmetrical behavior of allene under $\mathbf{D}_{2d}$. The feature of the reduced mandala is characterized by a simplified reduced mandala (**10**), which shows that the assembly ($\mathcal{G}_1^*$) of the eight identical transformulas (**2**–**9**, i.e., f_1–f_8) represents a single $\mathbf{D}_{2d}$-molecule (i.e., allene). It follows that the one-membered orbit $\mathcal{G}^*$ ($= \{\mathcal{G}_1^*\}$) is governed by the CR $\mathbf{D}_{2d}(/\mathbf{D}_{2d})$. Because the one-membered $\mathbf{D}_{2d}(/\mathbf{D}_{2d})$-orbit is fixed by any subgroups of $\mathbf{D}_{2d}$, the orbit for representing an allene molecule is characterized by marks $(1,1,1,1,1,1,1,1)$, where the marks, i.e., the number of fixed molecules (or assemblies for a reduced mandala in general), are aligned in the order of the SSG (eq. 1). Such an alignment of marks is called *a fixed-point vector* (FPV) according to the terminology of Fujita's book [6], because fixed molecules or fixed assemblies in a reduced mandala (Part 2) as well as fixed substitution positions in a molecule (Part 1) can be commonly regarded as fixed points contained in an abstract structure (e.g., the reduced mandala, the molecule, etc.).

Column View for $\mathbf{D}_{2d}$-Molecules. By keeping the USCI-CF (a_4) in mind (the top of the $\downarrow \mathbf{D}_{2d}$-column in Table 1), let us examine cases in which four substituents are selected from achiral ligands (H and X) and a pair of enantiomeric chiral ligands (p and $\overline{\mathrm{p}}$). Because of the homosphericity (Table 5 of Part 1), the $\mathbf{D}_{2d}(/\mathbf{C}_s)$-orbit accommodates achiral ligands only (Table 2 of Part 1). The following functions generate $\mathbf{D}_{2d}$-molecules that are suitable for the diagrammatical expression (**11**) selected from the reduced mandala (**10**).

2 (H^4) $f(1) = \mathrm{H}$, $f(2) = \mathrm{H}$, $f(3) = \mathrm{H}$, and $f(4) = \mathrm{H}$
12 (X^4) $f(1) = \mathrm{X}$, $f(2) = \mathrm{X}$, $f(3) = \mathrm{X}$, and $f(4) = \mathrm{X}$

The concrete forms are shown in Fig. 3.

The USCI-CF (a_4) corresponding to the subduction $\mathbf{D}_{2d}(/\mathbf{C}_s) \downarrow \mathbf{D}_{2d} = \mathbf{D}_{2d}(/\mathbf{C}_s)$ (cf. **11** shown in Fig. 3) indicates that the four substitution positions accommodate four achiral ligands of the same kind, i.e., four H's or four X's for the present case. Hence, we find the following equation:

$$a_4 = \mathrm{H}^4 + \mathrm{X}^4, \tag{2}$$

[3] The modes of numbering for f_1–f_8 have been discussed in Part 2.

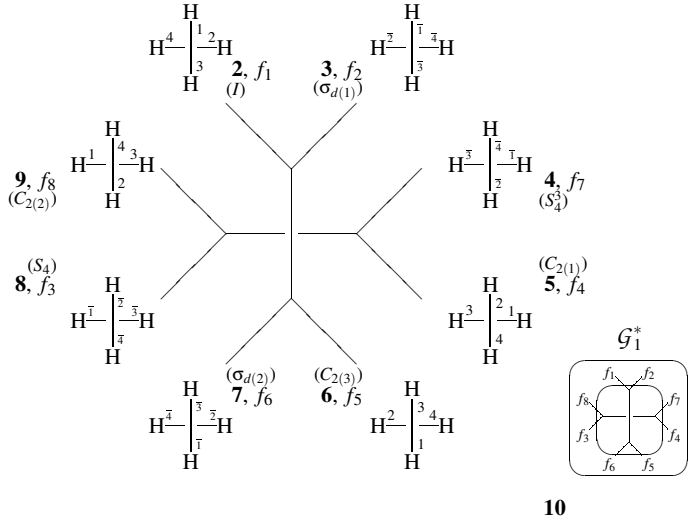

Figure 2: Reduced mandala with $\mathbf{D}_{2d}$-transformulas derived from an allene skeleton, the vertices of which construct an orbit governed by the CR $\mathbf{D}_{2d}(/\mathbf{C}_s)$. Because the eight $\mathbf{D}_{2d}$-transformulas are equivalent under $\mathbf{D}_{2d}$ so as to construct an eight-membered assembly, the resulting assembly constructs a one-membered orbit governed by the CR $\mathbf{D}_{2d}(/\mathbf{D}_{2d})$. The orbit (representing an allene molecule) is characterized by a fixed-point vector: $(1,1,1,1,1,1,1,1)$.

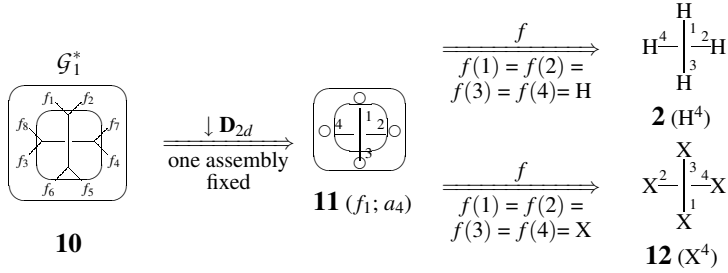

Figure 3: $\mathbf{D}_{2d}$-Molecules (**2** and **12**) on the reduced mandala with $\mathbf{D}_{2d}$-assemblage (**10**). The transformulas f_1–f_8 are so equivalent as to give an appropriate one (e.g., f_1; **11**) as a representative, which is transformed into **2** or **12** by a respective function f.

which is called *a ligand inventory*. In the present case, the ligand inventory is identical with the generating function for evaluating marks of the $\downarrow \mathbf{D}_{2d}$-column. Hence, the mark 1 appearing at the intersection of the $\mathbf{D}_{2d}(/\mathbf{D}_{2d})$-row and the $\downarrow \mathbf{D}_{2d}$-column (Table 1) indicates $1 \times \mathrm{H}^4$ or $1 \times \mathrm{X}^4$ for $\mathbf{D}_{2d}$-molecules. Note that the local symmetry ($\mathbf{D}_{2d}$) appearing in the CR $\mathbf{D}_{2d}(/\mathbf{D}_{2d})$ represents the symmetry of molecules enumerated, which are shown as **2** and **12** in Fig. 3.

2.2.2 $\mathbf{C}_s$-Molecules

Row View for $\mathbf{C}_s$-Molecules. The derivation of a mono-X-substituted molecule of $\mathbf{C}_s$-symmetry (**13**) is regarded as the action of another function f, where we place $f(1) = \mathrm{X}$, $f(2) = \mathrm{H}$, $f(3) = \mathrm{H}$, and $f(4) = \mathrm{H}$ (Fig. 4). The action of the symmetry operations of $\mathbf{D}_{2d}$ transforms **13** (f_1) into the transformulas (**13**–**20**, i.e., f_1–f_8), which generate a reduced mandala shown in Fig. 4. Obviously, the transformulas **13** and **14** are identical with each other so as to generate an assembly, which is regarded as a single $\mathbf{C}_s$-molecule. On the same line, the assembly of **15/16**, the assembly of **17/18**, and the assembly of **19/20** represent respective $\mathbf{C}_s$-molecules. In other words, the reduced mandala (Fig. 4) is spontaneously assembled to give the four assemblies, i.e., $\{f_1, f_2\}$ (**13/14**), $\{f_7, f_4\}$ (**15/16**), $\{f_5, f_6\}$ (**17/18**), and $\{f_3, f_8\}$ (**19/20**), each of which represents a $\mathbf{C}_s$-molecule permuted under $\mathbf{D}_{2d}$. The set of the four $\mathbf{C}_s$-assemblies constructs an orbit governed by the CR $\mathbf{D}_{2d}(/\mathbf{C}_s)$, as shown in **21**.

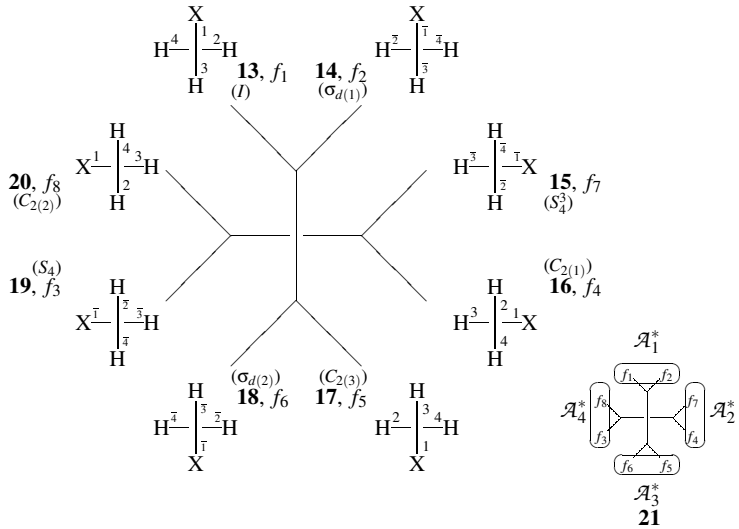

Figure 4: Reduced mandala with $\mathbf{C}_s$-transformulas derived from an allene skeleton, where a spontaneous assemblage occurs, as shown in a simplified assembly (**21**). Thus, the $\mathbf{C}_s$-transformulas are spontaneously assembled into four assemblies (**13/14**, **15/16**, **17/18**, and **19/20**), which construct a four-membered orbit governed by the CR $\mathbf{D}_{2d}(/\mathbf{C}_s)$. The orbit (representing a mono-X-allene molecule) is characterized by a fixed-point vector: $(4,0,0,2,0,0,0,0)$.

In order to characterize the four-membered $\mathbf{D}_{2d}(/\mathbf{C}_s)$-orbit appearing in the reduced mandala shown in Fig. 4, the simplified reduced mandala (**21**) is fixed (desymmetrized) by each subgroup of $\mathbf{D}_{2d}$, where the number (mark) of fixed assemblies among $\mathcal{A}_1^*$–$\mathcal{A}_4^*$ is evaluated diagrammatically, as has been already discussed in Part 2. Thereby, an FPV $(4,0,0,2,0,0,0,0)$ is obtained by aligning the resulting numbers (marks) in the order of the SSG (eq. 1).

The fixation process for obtaining the FPV corresponds to the subduction $\mathbf{D}_{2d}(/\mathbf{C}_s) \downarrow \mathbf{K}$, where the subgroup $\mathbf{K}$ covers the SSG (eq. 1). As an example, let us study the subduction $\mathbf{D}_{2d}(/\mathbf{C}_s) \downarrow \mathbf{C}_s$ (i.e., $\mathbf{K} = \mathbf{C}_s$) by using the simplified reduced mandala (**21**). The four-membered $\mathbf{D}_{2d}(/\mathbf{C}_s)$-orbit ($\mathcal{A}^* = \{\mathcal{A}_1^*, \mathcal{A}_2^*, \mathcal{A}_3^*, \mathcal{A}_4^*)\}$) is fixed in accord with the subduction $\mathbf{D}_{2d}(/\mathbf{C}_s) \downarrow \mathbf{C}_s$. Thereby, the original orbit $\mathcal{A}^*$ is divided into three suborbits, i.e., $\{\mathcal{A}_1^*\}$, $\{\mathcal{A}_2^*, \mathcal{A}_4^*\}$, and $\{\mathcal{A}_3^*\}$. Because the two assemblies, i.e., $\mathcal{A}_1^*$ and $\mathcal{A}_3^*$, are fixed as one-membered suborbits, the corresponding mark is obtained to be equal to 2, which appears as the fourth element of the FPV $(4,0,0,2,0,0,0,0)$. Let us represent this fact by the symbol $2\mathrm{H}^3\mathrm{X}$, where the coefficient represents the mark and the $\mathrm{H}^3\mathrm{X}$ represents the mode of substitution.[4] As for the full expression of the reduced mandala (Fig. 4), this fact corresponds to the fixation of $\{f_1, f_2\}$ (**13/14**) and $\{f_5, f_6\}$ (**17/18**), where the symmetrical meaning is obvious because of $\mathbf{C}_s = \{I, \sigma_{d(2)}\}$.

Fixation and $\mathbf{C}_s$-Molecules. The fixation process can be demonstrated more systematically by the diagram shown in Fig. 5, so that the process can be extended so as to be applicable to general cases other than $\mathrm{H}^3\mathrm{X}$. The reduced mandala (**21**), in which an abstract $\mathbf{C}_s$-assemblage (generally an $\mathbf{H}$-assemblage for a $\mathbf{G}(/\mathbf{H})$-orbit) generates the $\mathbf{D}_{2d}(/\mathbf{C}_s)$-orbit ($\mathcal{A}^* = \{\mathcal{A}_1^*, \mathcal{A}_2^*, \mathcal{A}_3^*, \mathcal{A}_4^*)\}$), is fixed by $\mathbf{C}_s$ in accord with the subduction $\mathbf{D}_{2d}(/\mathbf{C}_s) \downarrow \mathbf{C}_s$ (generally $\mathbf{G}(/\mathbf{H}) \downarrow \mathbf{K}$ where $\mathbf{K} = \mathbf{H}$). Thereby, the assemblies ($\mathcal{A}_1^*$ and $\mathcal{A}_3^*$) are fixed (i.e., mark = 2).

The assemblies ($\mathcal{A}_1^*$ and $\mathcal{A}_3^*$) selected by the fixation correspond to the transformulas **22** and **23**. Because the four vertices (substitution positions) of each transformula originally construct an $\mathbf{D}_{2d}(/\mathbf{C}_s)$-orbit (generally $\mathbf{G}(/\mathbf{H}')$), the fixation (desymmetrization) causes the subduction $\mathbf{D}_{2d}(/\mathbf{C}_s) \downarrow \mathbf{C}_s$ (generally $\mathbf{G}(/\mathbf{H}') \downarrow \mathbf{H}$). As a result, the original CR $\mathbf{D}_{2d}(/\mathbf{C}_s)$ for allene suffers from the subduction represented by $\mathbf{D}_{2d}(/\mathbf{C}_s) \downarrow \mathbf{C}_s = 2\mathbf{C}_s(/\mathbf{C}_s) + \mathbf{C}_s(/\mathbf{C}_1)$ (cf. Part 1). Thus, the orbit of the four substitution positions (vertices) is divided into three suborbits, i.e., $\{1\}$, $\{2,4\}$, and $\{3\}$, as shown in **22** and **23**.[5] Because the one-membered orbit $\mathbf{C}_s(/\mathbf{C}_s)$ is homospheric (the sphericity index: a_1 for position 1 or position 3) and the two-membered orbit $\mathbf{C}_s(/\mathbf{C}_1)$ is enantiospheric (the sphericity index: c_2 for positions 2 and 4), we can obtain $a_1^2 c_2$ as the corresponding unit-subduced-cycle-index with chirality fittingness (USCI-CF). The chirality fittingness due to each sphericity index appearing in the USCI-CF (Table 2 of Part 1) permits the accommodation represented by the function f, i.e., $f(1) = \mathrm{X}$, $f(2) = \mathrm{H}$, $f(3) = \mathrm{H}$, and $f(4) = \mathrm{H}$. As a result, **22** and **23** are respectively converted into **13** and **17**, which are equivalent under $\mathbf{D}_{2d}$ but counted distinctly as two fixed molecules (assemblies), so that the mark for $\mathbf{D}_{2d}(/\mathbf{C}_s) \downarrow \mathbf{C}_s$ (generally $\mathbf{G}(/\mathbf{H}) \downarrow \mathbf{K}$ where $\mathbf{K} = \mathbf{H} = \mathbf{C}_s$) is determined to be 2.

Because the transformulas (**22** and **23**) exhibit the same division of vertices without taking the modes of numbering into consideration, either one (e.g., **22**) is selected so as to give **13** and **17** by using different functions, f and f', where we place f: $f(1) = \mathrm{X}$, $f(2) = \mathrm{H}$, $f(3) = \mathrm{H}$,

[4] In chemistry, a molecular formula is usually written by expressing atom numbers as subscripts (e.g., $\mathrm{H_3X}$). The present paper adopts superscript expressions (e.g., $\mathrm{H}^3\mathrm{X}$), because generating functions used in the present paper involve monomial terms due to such superscript expressions.

[5] In Part 1, the orbit of vertices is correlated to the orbit of segments, i.e., $\mathcal{A}$ (= $\{\mathcal{A}_1, \mathcal{A}_2, \mathcal{A}_3, \mathcal{A}_4)\}$), which is governed by the CR $\mathbf{D}_{2d}(/\mathbf{C}_s)$. For the sake of simplicity, the orbit $\mathcal{A}$ is equalized to the set of locants, i.e., $\{1,2,3,4\}$.

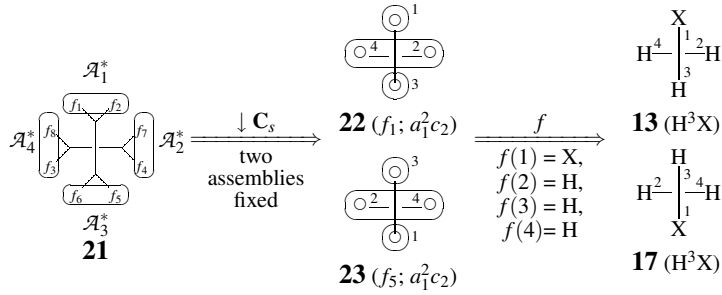

Figure 5: $\mathbf{C}_s$-Molecules (**13** and **17**) on the reduced mandala with $\mathbf{C}_s$-assemblage (**21**). The intermediate transformulas (**22** and **23**) are selected as fixed (abstract) points in accord with the mark (= 2) for the subduction $\mathbf{D}_{2d}(/\mathbf{C}_s) \downarrow \mathbf{C}_s = 2\mathbf{C}_s(/\mathbf{C}_s) + \mathbf{C}_s(/\mathbf{C}_1)$, which is concerned with the reduced mandala (**21**). On the other hand, each of the transformulas (**22** and **23**) shows the mode of substitution in a molecule, which is a diagrammatical expression of the subduction represented by $\mathbf{D}_{2d}(/\mathbf{C}_s) \downarrow \mathbf{C}_s = 2\mathbf{C}_s(/\mathbf{C}_s) + \mathbf{C}_s(/\mathbf{C}_1)$.

and $f(4) = \mathrm{H}$; and f': $f'(1) = \mathrm{H}$, $f'(2) = \mathrm{H}$, $f'(3) = \mathrm{X}$, and $f'(4) = \mathrm{H}$.

Column View for $\mathbf{C}_s$-Molecules. By keeping the USCI-CF ($a_1^2c_2$) in mind, let us examine cases in which four substituents are selected from achiral ligands (H and X) and a pair of enantiomeric chiral ligands (p and $\overline{\mathrm{p}}$). The following functions generate $\mathbf{C}_s$-molecules that are suitable for the diagrammatical expression (**22**) selected from the reduced mandala (**21**).

13	($2H^3X$)	$f(1) = \mathrm{X}$, $f(2) = \mathrm{H}$, $f(3) = \mathrm{H}$, and $f(4) = \mathrm{H}$
24	($2H^2p\overline{p}$)	$f(1) = \mathrm{H}$, $f(2) = \overline{\mathrm{p}}$, $f(3) = \mathrm{H}$, and $f(4) = \mathrm{p}$
25	($2HXp\overline{p}$)	$f(1) = \mathrm{X}$, $f(2) = \overline{\mathrm{p}}$, $f(3) = \mathrm{H}$, and $f(4) = \mathrm{p}$
26	($2HX^3$)	$f(1) = \mathrm{H}$, $f(2) = \mathrm{X}$, $f(3) = \mathrm{X}$, and $f(4) = \mathrm{X}$
27	($2X^2p\overline{p}$)	$f(1) = \mathrm{X}$, $f(2) = \overline{\mathrm{p}}$, $f(3) = \mathrm{X}$, and $f(4) = \mathrm{p}$
28	($2HXp\overline{p}$)	$f(1) = \mathrm{X}$, $f(2) = \mathrm{p}$, $f(3) = \mathrm{H}$, and $f(4) = \overline{\mathrm{p}}$

The concrete forms of these $\mathbf{C}_s$-molecules are depicted in Fig. 6, where one (**22**) of the transformulas and one function f are used for the sake of simplicity. Hence, each $\mathbf{C}_s$-molecule shown in Fig. 6 corresponds to two fixed assemblies (mark = 2), which are represented by the coefficient 2 in the symbol for designating the mode of substitution (e.g., $2H^3X$ for **13**).

According to the chirality fittingness defined in Fujita's USCI approach (Table 2 of Part 1), an enantiospheric orbit permits two modes of pairwise packing in which one half of the enantiospheric orbit can accommodate chiral ligands of the same kind and the remaining half can accommodate their enantiomeric ligands. Among the $\mathbf{C}_s$-molecules listed in Fig. 6, the transformulas **25** and **28**, both of which corresponds to $2HXp\overline{p}$, represent two modes of such pairwise packing. The two modes of pairwise packing (for p and $\overline{\mathrm{p}}$) in **24** (or **27**) are equalized symmetrically so as to give a single $\mathbf{C}_s$-molecule.

Each one-membered homospheric orbit (a_1 appearing in $a_1^2c_2$) can accommodate H or X. The two modes of pairwise packing for the enantiospheric orbit (c_2 appearing in $a_1^2c_2$) are

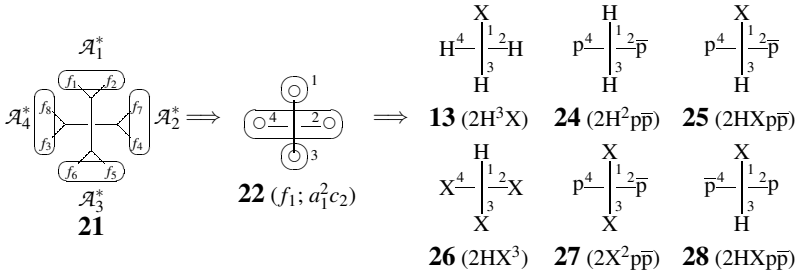

Figure 6: $\mathbf{C}_s$-Molecules (**13**, **24**–**28**) on the reduced mandala with $\mathbf{C}_s$-assemblage (**21**). The modes of substitution in the $\mathbf{C}_s$-molecules are represented by **22**, which is a diagrammatical expression of the subduction represented by $\mathbf{D}_{2d}(/\mathbf{C}_s) \downarrow \mathbf{C}_s = 2\mathbf{C}_s(/\mathbf{C}_s) + \mathbf{C}_s(/\mathbf{C}_1)$.

represented by the term 2p$\overline{\text{p}}$. It follows that the ligand inventories for this case are obtained as follows:

$$a_1 = \text{H} + \text{X} \tag{3}$$
$$c_2 = \text{H}^2 + \text{X}^2 + 2\text{p}\overline{\text{p}} \tag{4}$$

Because the modes of accommodation due to terms a_1, a_1, and c_2 take place independently, the generating function for evaluating marks of the $\downarrow \mathbf{C}_s$-column is obtained as follows:

$$\begin{aligned} a_1^2c_2 &= (\text{H}+\text{X})^2(\text{H}^2+\text{X}^2+2\text{p}\overline{\text{p}}) \\ &= (\text{H}^4+\text{X}^4)+(2\text{H}^3\text{X}+2\text{HX}^3)+2\text{H}^2\text{X}^2+2\text{H}^2\text{p}\overline{\text{p}}+2\text{X}^2\text{p}\overline{\text{p}}+4\text{HXp}\overline{\text{p}} \end{aligned} \tag{5}$$

Among the terms appearing in eq. 5, the term H^4 (or X^4) is concerned with the mark (1) for a $\mathbf{D}_{2d}$-molecule, which appears at the intersection of the $\mathbf{C}_s$-column and the $\mathbf{D}_{2d}(/\mathbf{D}_{2d})$-row of the mark table (Table 1). The term 2H^{2}X^2 is concerned with the mark (2) for a $\mathbf{C}_{2v}$-molecule, which appears at the intersection of the $\mathbf{C}_s$-column and the $\mathbf{D}_{2d}(/\mathbf{C}_{2v})$-row of Table 1. Remember the subgroup-supergroup relationships shown in Fig. 1.

On the other hand, the remaining terms appearing in the last part of eq. 5 are concerned with $\mathbf{C}_s$-molecules, each of which corresponds to the coefficient of the term at issue. Thus, the mark (2) appearing at the intersection of the $\mathbf{D}_{2d}(/\mathbf{C}_s)$-row and the $\downarrow \mathbf{C}_s$-column (Table 1) can be related to the coefficients of these terms: 2H^{3}X (**13**), 2HX^3 (**26**), 2H^{2}p$\overline{\text{p}}$ (**24**), 2X^{2}p$\overline{\text{p}}$ (**27**), and 4HXp$\overline{\text{p}}$ (**25** and **28**).

2.2.3 $\mathbf{C}_2'$-Molecules

Row View for $\mathbf{C}_2'$-Molecules. Let us consider the action of a function f, where we place $f(1) = \text{X}$, $f(2) = \text{X}$, $f(3) = \text{H}$, and $f(4) = \text{H}$ (Fig. 7). This function generates a di-X-substituted allene derivative of $\mathbf{C}_2'$-symmetry (**29**). A reduced mandala shown in Fig. 7 is generated by the symmetry operations of $\mathbf{D}_{2d}$, which transform **29** (f_1) into the transformulas (**29**–**36**, i.e., f_1–f_8). As found easily, the reduced mandala (Fig. 7) is spontaneously assembled to give four assemblies, $\{f_1, f_4\}$ (**29/32**), $\{f_2, f_3\}$ (**30/35**), $\{f_5, f_8\}$ (**33/36**), and $\{f_6, f_7\}$ (**31/34**), each of which represents a $\mathbf{C}_2'$-molecule permuted under $\mathbf{D}_{2d}$. The set of the four assemblies constructs an orbit governed by the CR $\mathbf{D}_{2d}(/\mathbf{C}_2')$, as shown in **37**, where we place $\mathbf{G} = \mathbf{D}_{2d}$ and $\mathbf{H} = \mathbf{C}_2'$.

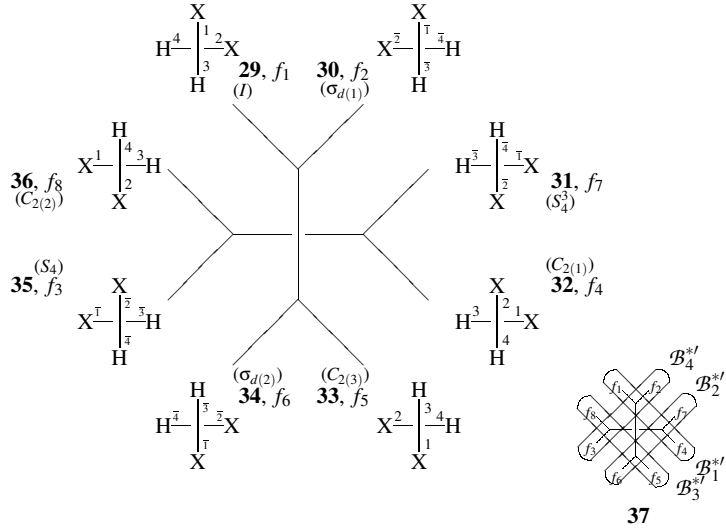

Figure 7: Reduced mandala with $\mathbf{C}_2'$-transformulas derived from an allene skeleton, the vertices of which construct an orbit governed by the subduction of the CR $\mathbf{D}_{2d}(/\mathbf{C}_s) \downarrow \mathbf{C}_2' = 2\mathbf{C}_2'(/\mathbf{C}_1)$. The $\mathbf{C}_2'$-transformulas are assembled into four assemblies (**29/32**, **33/36**, **30/35**, and **31/34**), which construct a four-membered orbit governed by the CR $\mathbf{D}_{2d}(/\mathbf{C}_2')$. The orbit (representing a di-X-allene molecule) is characterized by marks $(4,0,2,0,0,0,0,0)$.

The reduced mandala shown in Fig. 7 is converted into the simplified reduced mandala (**37**), where we place $\mathcal{B}_1^{*\prime} = \{f_1, f_4\}$ (**29/32**), $\mathcal{B}_4^{*\prime} = \{f_2, f_3\}$ (**30/35**), $\mathcal{B}_3^{*\prime} = \{f_5, f_8\}$ (**33/36**), and $\mathcal{B}_2^{*\prime} = \{f_6, f_7\}$ (**31/34**) (cf. Fig. 14 in Part 2). Then, the simplified reduced mandala is fixed (desymmetrized) by each subgroup of $\mathbf{D}_{2d}$ in order to characterize the four-membered $\mathbf{D}_{2d}(/\mathbf{C}_2')$-orbit, i.e., $\mathcal{B}^{*\prime} = \{\mathcal{B}_1^{*\prime}, \mathcal{B}_2^{*\prime}, \mathcal{B}_3^{*\prime}, \mathcal{B}_4^{*\prime}\}$. The number (mark) of fixed assemblies among $\mathcal{B}_1^{*\prime}$–$\mathcal{B}_4^{*\prime}$ is evaluated diagrammatically, as has been already discussed in Part 2. Thereby, an FPV $(4,0,2,0,0,0,0,0)$ is obtained by aligning the resulting numbers (marks) in the order of the SSG (eq. 1).

The fixation process for obtaining the FPV corresponds to the subduction $\mathbf{D}_{2d}(/\mathbf{C}_2') \downarrow \mathbf{H}$, where the subgroup $\mathbf{H}$ is selected from the SSG (eq. 1). For example, the subduction $\mathbf{D}_{2d}(/\mathbf{C}_2') \downarrow \mathbf{C}_2'$ causes the fixation of the four-membered $\mathbf{D}_{2d}(/\mathbf{C}_2')$-orbit ($\mathcal{B}^{*\prime}$) in the simplified reduced mandala (**37**). Thereby, the orbit $\mathcal{B}^{*\prime}$ is restricted within $\mathbf{C}_2'$ so as to be divided into three suborbits, i.e., $\{\mathcal{B}_1^{*\prime}\}$, $\{\mathcal{B}_2^{*\prime}, \mathcal{B}_4^{*\prime}\}$, and $\{\mathcal{B}_3^{*\prime}\}$. Because the two assemblies, i.e., $\mathcal{B}_1^{*\prime}$ and $\mathcal{B}_3^{*\prime}$, are fixed as one-membered suborbits, the corresponding mark is determined to be equal to 2, which appears as the third element of the FPV $(4,0,2,0,0,0,0,0)$. This fact is designated by the symbol $2H^2X^2$.

Fixation and $\mathbf{C}_2'$-Molecules. The diagram shown in Fig. 8 shows the effect of the fixation process more systematically by considering the relationship between the subduction $\mathbf{D}_{2d}(/\mathbf{C}_2') \downarrow \mathbf{C}_2'$

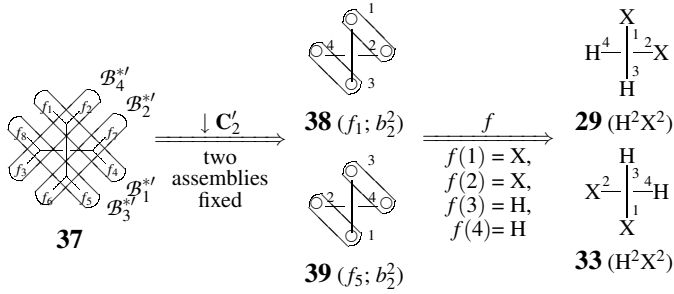

Figure 8: $\mathbf{C}_2'$-Molecules (**29** and **33**) on the reduced mandala with $\mathbf{C}_2'$-assemblage (**37**). The intermediate transformulas (**38** and **39**) are selected as fixed (abstract) points in accord with the mark (= 2) for the subduction $\mathbf{D}_{2d}(/\mathbf{C}_2') \downarrow \mathbf{C}_2' = 2\mathbf{C}_2'(/\mathbf{C}_2') + \mathbf{C}_2'(/\mathbf{C}_1)$, which is concerned with the reduced mandala (**37**). On the other hand, each of the transformulas (**38** and **39**) shows the mode of substitution in a molecule, which is a diagrammatical expression of the subduction represented by $\mathbf{D}_{2d}(/\mathbf{C}_s) \downarrow \mathbf{C}_2' = 2\mathbf{C}_2'(/\mathbf{C}_1)$.

(for the reduced mandala **37**) and the subduction $\mathbf{D}_{2d}(/\mathbf{C}_s) \downarrow \mathbf{C}_2'$ (for transformulas contained in **37**). According to the former subduction, the orbit $\mathcal{B}^{*\prime}$ (= $\{\mathcal{B}_1^{*\prime}, \mathcal{B}_2^{*\prime}, \mathcal{B}_3^{*\prime}, \mathcal{B}_4^{*\prime}\}$) is desymmetrized to make two assemblies ($\mathcal{B}_1^{*\prime}$ and $\mathcal{B}_3^{*\prime}$) fixed. From the fixed assemblies ($\mathcal{B}_1^{*\prime}$ and $\mathcal{B}_3^{*\prime}$), the transformulas **29** and **33** are depicted as representatives in Fig. 8. Because the four vertices (substitution positions) of each transformula originally construct an $\mathbf{D}_{2d}(/\mathbf{C}_s)$-orbit, the fixation (desymmetrization) causes the latter subduction $\mathbf{D}_{2d}(/\mathbf{C}_s) \downarrow \mathbf{C}_2'$. As a result, the original CR $\mathbf{D}_{2d}(/\mathbf{C}_s)$ for allene suffers from the subduction represented by $\mathbf{D}_{2d}(/\mathbf{C}_s) \downarrow \mathbf{C}_2' = 2\mathbf{C}_2'(/\mathbf{C}_1)$ (cf. Part 1). Thus, the orbit of the four substitution positions (vertices) is divided into two suborbits, i.e., $\{1,2\}$ and $\{3,4\}$, as shown in **38** and **39**.

Because each two-membered orbit $\mathbf{C}_2'(/\mathbf{C}_1)$ is hemispheric (the sphericity index: b_2 for positions $\{1,2\}$ or positions $\{3,4\}$), we can obtain b_2^2 as the corresponding USCI-CF. The chirality fittingness due to each sphericity index appearing in the USCI-CF (Table 2 of Part 1) permits the accommodation represented by the function f, i.e., $f(1) = \mathrm{X}$, $f(2) = \mathrm{X}$, $f(3) = \mathrm{H}$, and $f(4) = \mathrm{H}$. As a result, **38** and **39** are respectively converted into **29** and **33**. These are equivalent under $\mathbf{D}_{2d}$ but counted distinctly as two fixed molecules (assemblies), so that the mark for $\mathbf{D}_{2d}(/\mathbf{C}_2') \downarrow \mathbf{C}_2'$ is determined to be 2.

The treatment described for Fig. 8 can be alternatively discussed by using either one of the transformulas **38** and **39**, because they exhibit the same division of vertices without taking the modes of numbering into consideration. Thus, **29** and **33** are alternatively obtained by selecting **38** and by using different functions, f and f', where we place f: $f(1) = \mathrm{X}$, $f(2) = \mathrm{H}$, $f(3) = \mathrm{H}$, and $f(4) = \mathrm{H}$; and f': $f'(1) = \mathrm{H}$, $f'(2) = \mathrm{H}$, $f'(3) = \mathrm{X}$, and $f'(4) = \mathrm{H}$.

Column View for $\mathbf{C}_2'$-Molecules. Let us examine cases in which four substituents are selected from achiral ligands (H and X) and a pair of enantiomeric chiral ligands (p and $\overline{\mathrm{p}}$). By keeping the USCI-CF (b_2^2) in mind, the following functions generate $\mathbf{C}_2'$-molecules that are suitable for the diagrammatical expression (**38**) selected from the reduced mandala (**37**).

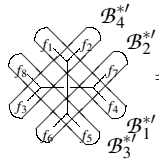

37

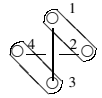

38 $(f_1; b_2^2)$

$\mathrm{H}^4\!\left|\begin{smallmatrix}\mathrm{X}\\ 1\\ 2\\ 3\\ \mathrm{H}\end{smallmatrix}\right.\!\mathrm{X}$ **29** $(2\mathrm{H}^2\mathrm{X}^2)$ $\quad$ $\mathrm{H}^4\!\left|\begin{smallmatrix}\mathrm{p}\\ 1\\ 2\\ 3\\ \mathrm{H}\end{smallmatrix}\right.\!\mathrm{p}$ **40** $(2\mathrm{H}^2\mathrm{p}^2)$ $\quad$ $\mathrm{H}^4\!\left|\begin{smallmatrix}\overline{\mathrm{p}}\\ 1\\ 2\\ 3\\ \mathrm{H}\end{smallmatrix}\right.\!\overline{\mathrm{p}}$ **41** $(2\mathrm{H}^2\overline{\mathrm{p}}^2)$

$\overline{\mathrm{p}}^4\!\left|\begin{smallmatrix}\mathrm{p}\\ 1\\ 2\\ 3\\ \overline{\mathrm{p}}\end{smallmatrix}\right.\!\mathrm{p}$ **42** $(2\mathrm{p}^2\overline{\mathrm{p}}^2)$ $\quad$ $\mathrm{X}^4\!\left|\begin{smallmatrix}\mathrm{p}\\ 1\\ 2\\ 3\\ \mathrm{X}\end{smallmatrix}\right.\!\mathrm{p}$ **43** $(2\mathrm{X}^2\mathrm{p}^2)$ $\quad$ $\mathrm{X}^4\!\left|\begin{smallmatrix}\overline{\mathrm{p}}\\ 1\\ 2\\ 3\\ \mathrm{X}\end{smallmatrix}\right.\!\overline{\mathrm{p}}$ **44** $(2\mathrm{X}^2\overline{\mathrm{p}}^2)$

Figure 9: $\mathbf{C}_2'$-Molecules (**29**, **40**–**44**) on the reduced mandala with $\mathbf{C}_2'$-assemblage (**37**). The modes of substitution in the $\mathbf{C}_2'$-molecules are represented by **38**, which is a diagrammatical expression of the subduction represented by $\mathbf{D}_{2d}(/\mathbf{C}_s) \downarrow \mathbf{C}_2' = 2\mathbf{C}_2'(/\mathbf{C}_1)$.

29	$(2\mathrm{H}^2\mathrm{X}^2)$	$f(1) = \mathrm{X}$, $f(2) = \mathrm{X}$, $f(3) = \mathrm{H}$, and $f(4) = \mathrm{H}$
40	$(2\mathrm{H}^2\mathrm{p}^2)$	$f(1) = \mathrm{p}$, $f(2) = \mathrm{p}$, $f(3) = \mathrm{H}$, and $f(4) = \mathrm{H}$
41	$(2\mathrm{H}^2\overline{\mathrm{p}}^2)$	$f(1) = \overline{\mathrm{p}}$, $f(2) = \overline{\mathrm{p}}$, $f(3) = \mathrm{H}$, and $f(4) = \mathrm{H}$
42	$(2\mathrm{p}^2\overline{\mathrm{p}}^2)$	$f(1) = \mathrm{p}$, $f(2) = \mathrm{p}$, $f(3) = \overline{\mathrm{p}}$, and $f(4) = \overline{\mathrm{p}}$
43	$(2\mathrm{X}^2\mathrm{p}^2)$	$f(1) = \mathrm{p}$, $f(2) = \mathrm{p}$, $f(3) = \mathrm{X}$, and $f(4) = \mathrm{X}$
44	$(2\mathrm{X}^2\overline{\mathrm{p}}^2)$	$f(1) = \overline{\mathrm{p}}$, $f(2) = \overline{\mathrm{p}}$, $f(3) = \mathrm{X}$, and $f(4) = \mathrm{X}$

The concrete forms of these $\mathbf{C}_2'$-molecules are depicted in Fig. 9, where one (**38**) of the transformulas and one function f are used for the sake of simplicity. It follows that each $\mathbf{C}_2'$-molecule shown in Fig. 9 corresponds to two fixed assemblies (mark = 2), which are represented by the coefficient 2 in the symbol for designating the mode of substitution (e.g., the coefficient 2 appearing in $2\mathrm{H}^2\mathrm{X}^2$ for **29**).

Each two-membered hemispheric orbit (b_2 appearing in b_2^2) can accommodate two ligands of the same kind, which are selected from H, X, p, and $\overline{\mathrm{p}}$. Hence, the ligand inventory for this case is obtained as follows:

$$b_2 = \mathrm{H}^2 + \mathrm{X}^2 + \mathrm{p}^2 + \overline{\mathrm{p}}^2 \tag{6}$$

Because the modes of accommodation due to the two terms (b_2) take place independently, the generating function for evaluating marks of the $\downarrow \mathbf{C}_2'$-column is obtained as follows:

$$\begin{aligned} b_2^2 &= (\mathrm{H}^2 + \mathrm{X}^2 + \mathrm{p}^2 + \overline{\mathrm{p}}^2)^2 \\ &= (\mathrm{H}^4 + \mathrm{X}^4) + 2\mathrm{H}^2\mathrm{X}^2 \\ &\quad + 2 \times \frac{1}{2}(\mathrm{p}^4 + \overline{\mathrm{p}}^4) + 4 \times \frac{1}{2}(\mathrm{H}^2\mathrm{p}^2 + \mathrm{H}^2\overline{\mathrm{p}}^2) + 4 \times \frac{1}{2}(\mathrm{X}^2\mathrm{p}^2 + \mathrm{X}^2\overline{\mathrm{p}}^2) + 2\mathrm{p}^2\overline{\mathrm{p}}^2 \end{aligned} \tag{7}$$

Among the terms appearing in eq. 7, the term H^4 (or X^4) is concerned with the mark (1) for a $\mathbf{D}_{2d}$-molecule, which appears at the intersection of the $\mathbf{C}_2'$-column and the $\mathbf{D}_{2d}(/\mathbf{D}_{2d})$-row of the mark table (Table 1). The combined term $2 \times \frac{1}{2}(\mathrm{p}^4 + \overline{\mathrm{p}}^4)$ is concerned with the mark (2) for a $\mathbf{D}_2$-molecule, which appears at the intersection of the $\mathbf{C}_2'$-column and the $\mathbf{D}_{2d}(/\mathbf{D}_2)$-row of Table 1. Note that respective pairs of enantiomers are taken into consideration in the evaluation of marks.

The remaining terms appearing in eq. 5 are concerned with $\mathbf{C}_2'$-molecules, each of which corresponds to the coefficient of the term at issue. Thus, the mark (2) appearing at the intersection of the $\mathbf{D}_{2d}(/\mathbf{C}_2')$-row and the $\downarrow \mathbf{C}_2'$-column (Table 1) can be correlated to the coefficients of these terms: $2\mathrm{H}^2\mathrm{X}^2$ (**29**/its enantiomer),[6] $4 \times \frac{1}{2}(\mathrm{H}^2\mathrm{p}^2 + \mathrm{H}^2\overline{\mathrm{p}}^2)$ (the mark 2 for **40**/its enantiomer plus the mark 2 for **41**/its enantiomer), $4 \times \frac{1}{2}(\mathrm{X}^2\mathrm{p}^2 + \mathrm{X}^2\overline{\mathrm{p}}^2)$ (the mark 2 for **43**/its enantiomer plus the mark 2 for **44**/its enantiomer), and $2\mathrm{p}^2\overline{\mathrm{p}}^2$ (**42**/its enantiomer).

2.2.4 $\mathbf{C}_2$-Molecules

Row View for $\mathbf{C}_2$-Molecules. Let us consider a function f (i.e., $f(1) = \mathrm{p}$, $f(2) = \mathrm{H}$, $f(3) = \mathrm{p}$, and $f(4) = \mathrm{H}$), which is operated to the allene skeleton. This function generates a di-p-substituted allene derivative of $\mathbf{C}_2$-symmetry (**45**), as shown in Fig. 10. The corresponding reduced mandala (Fig. 10) is generated by the symmetry operations of $\mathbf{D}_{2d}$, which transform **45** (f_1) into the transformulas (**45**–**52**, i.e., f_1–f_8). As found easily, the reduced mandala (Fig. 10) is spontaneously assembled to give four assemblies, $\{f_1, f_5\}$ (**45/49**), $\{f_2, f_6\}$ (**46/50**), $\{f_7, f_3\}$ (**47/51**), and $\{f_4, f_8\}$ (**48/52**), each of which represents a $\mathbf{C}_2$-molecule permuted under $\mathbf{D}_{2d}$.

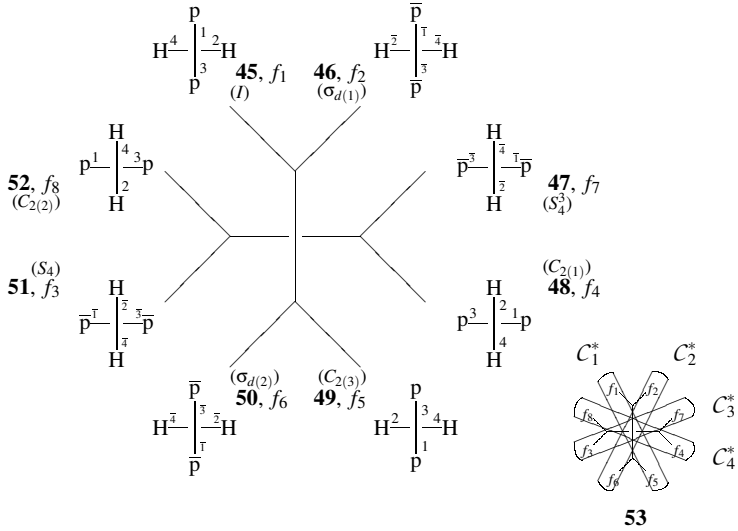

Figure 10: Reduced mandala with $\mathbf{C}_2$-transformulas derived from an allene skeleton, the vertices of which construct an orbit governed by the subduction of the CR $\mathbf{D}_{2d}(/\mathbf{C}_s) \downarrow \mathbf{C}_2 = 2\mathbf{C}_2(/\mathbf{C}_1)$. The $\mathbf{C}_2$-transformulas are assembled into four assemblies (**45/49**, **46/50**, **47/51**, and **48/52**), which construct a four-membered orbit governed by the CR $\mathbf{D}_{2d}(/\mathbf{C}_2)$. The orbit (representing a di-p-allene molecule) is characterized by marks $(4,4,0,0,0,0,0,0)$.

The set of the four assemblies constructs an orbit governed by the CR $\mathbf{D}_{2d}(/\mathbf{C}_2)$. Thus, the reduced mandala shown in Fig. 10 can be simplified to give a simplified reduced mandala (**53**)

[6] Strictly speaking, the combined term $2 \times \frac{1}{2}(\mathrm{H}^2\mathrm{X}^2 + \mathrm{H}^2\mathrm{X}^2)$ should be used.

by placing $\mathcal{C}_1^* = \{f_1, f_5\}$ (**45/49**), $\mathcal{C}_2^* = \{f_2, f_6\}$ (**46/50**), $\mathcal{C}_3^* = \{f_7, f_3\}$ (**47/51**), and $\mathcal{C}_4^* = \{f_4, f_8\}$ (**48/52**). Thereby, there emerges a four-membered $\mathbf{D}_{2d}(/\mathbf{C}_2)$-orbit, i.e., $\mathcal{C}^* = \{\mathcal{C}_1^*, \mathcal{C}_2^*, \mathcal{C}_3^*, \mathcal{C}_4^*\}$. The orbit $\mathcal{C}^*$ in the simplified reduced mandala (**53**) is fixed by the restriction into each subgroup of $\mathbf{D}_{2d}$, where the number (mark) of fixed assemblies among $\mathcal{C}_1^*$–$\mathcal{C}_4^*$ is evaluated diagrammatically, as has been already discussed in Part 2. Thereby, an FPV $(4,4,0,0,0,0,0,0)$ is obtained by aligning the resulting numbers (marks) in the order of the SSG (eq. 1).

The fixation process for obtaining the FPV corresponds to the subduction $\mathbf{D}_{2d}(/\mathbf{C}_2) \downarrow \mathbf{H}$, where the subgroup $\mathbf{H}$ is selected from the SSG (eq. 1). For example, the subduction $\mathbf{D}_{2d}(/\mathbf{C}_2) \downarrow \mathbf{C}_2$ causes the fixation of the two-membered $\mathbf{D}_{2d}(/\mathbf{C}_2)$-orbit ($\mathcal{C}^*$) in the simplified reduced mandala (**53**). Thereby, the four assemblies contained in the orbit $\mathcal{C}^*$ are forced to be non-equivalent so as to construct four one-membered suborbits. Hence, the corresponding mark is determined to be equal to 4, which appears as the second element of the FPV $(4,4,0,0,0,0,0,0)$. This fact is designated by the symbol $4 \times \frac{1}{2}(\mathrm{H}^2\mathrm{p}^2+\mathrm{H}^2\overline{\mathrm{p}}^2)$.[7]

Fixation and $\mathbf{C}_2$-Molecules. The effect of the fixation process is diagrammatically shown in Fig. 11 by using the subduction $\mathbf{D}_{2d}(/\mathbf{C}_2) \downarrow \mathbf{C}_2$ applied to the reduced mandala **53**. All of the assemblies $\mathcal{C}_1^*$–$\mathcal{C}_4^*$ contained in the orbit $\mathcal{C}^*$ are fixed, giving transformulas **54**–**57**, which are selected as representatives. Because the four vertices (substitution positions) of each transformula originally construct a $\mathbf{D}_{2d}(/\mathbf{C}_s)$-orbit, the fixation (desymmetrization) causes the subduction $\mathbf{D}_{2d}(/\mathbf{C}_s) \downarrow \mathbf{C}_2 = 2\mathbf{C}_2(/\mathbf{C}_1)$. Thereby, the orbit of the four substitution positions (vertices) is divided into two suborbits, i.e., $\{1,3\}$ and $\{2,4\}$, as shown in **54**–**57**. Because each two-membered orbit $\mathbf{C}_2(/\mathbf{C}_1)$ is hemispheric (the sphericity index: b_2 for positions $\{1,3\}$ or positions $\{2,4\}$), we can obtain b_2^2 as the corresponding USCI-CF. The chirality fittingness due to each sphericity index appearing in the USCI-CF (Table 2 of Part 1) permits the accommodation represented by the function f, i.e., $f(1) = \mathrm{p}$, $f(2) = \mathrm{H}$, $f(3) = \mathrm{p}$, and $f(4) = \mathrm{H}$. As a result, **54**–**55** are respectively converted into **45**, **46**, **48**, and **51**. These are equivalent under $\mathbf{D}_{2d}$ but counted distinctly as four fixed molecules (assemblies), so that the mark for $\mathbf{D}_{2d}(/\mathbf{C}_2) \downarrow \mathbf{C}_2$ is determined to be 4. It should be noted that **45** and **48** are equivalent to each other, while **46** and **51** and equivalent to each other. Although **45/48** and **46/51** are enantiomeric to each other, they are regarded as being equivalent under $\mathbf{D}_{2d}$. According to Fujita's USCI approach, each pair of enantiomers is counted once so that each of the four molecules (**45**, **46**, **48**, and **51**) is counted once to correspond to the term $\frac{1}{2}(\mathrm{H}^2\mathrm{p}^2+\mathrm{H}^2\overline{\mathrm{p}}^2)$. The mark (4) is considered as the coefficient of $4 \times \frac{1}{2}(\mathrm{H}^2\mathrm{p}^2+\mathrm{H}^2\overline{\mathrm{p}}^2)$, where the term $\frac{1}{2}(\mathrm{H}^2\mathrm{p}^2+\mathrm{H}^2\overline{\mathrm{p}}^2)$ is regarded as a unit term.[8]

Column View for $\mathbf{C}_2$-Molecules. Each two-membered hemispheric orbit (b_2 appearing in b_2^2) can accommodate two ligands of the same kind, which are selected from H, X, p, and $\overline{\mathrm{p}}$. Hence, the same ligand inventory as shown in eq. 6 can be used in this case. It follows that the same generating function as shown in eq. 7 can be used to evaluate marks of the $\downarrow \mathbf{C}_2$-column. Among the terms appearing in eq. 7, the term H^4 (or X^4) is concerned with the mark (1) for a $\mathbf{D}_{2d}$-molecule, which appears at the intersection of the $\mathbf{C}_2$-column and the $\mathbf{D}_{2d}(/\mathbf{D}_{2d})$-row of the mark table (Table 1). The combined term $2 \times \frac{1}{2}(\mathrm{p}^4+\overline{\mathrm{p}}^4)$ is concerned with the mark (2) for

[7] It should be noted that **45** and its enantiomer belong to the same $\mathbf{C}_2$-symmetry. On the other hand, **40** (Fig. 9) and its enantiomer belong respectively to $\mathbf{C}_2'$ and $\mathbf{C}_2''$, which are conjugate to each other. Because only $\mathbf{C}_2'$ is taken into consideration, **40** is permitted to be characterized by the term $2\mathrm{H}^2\mathrm{p}^2$, as described above. More strictly speaking, however, the $\mathbf{C}_2'$-case should be characterized by $2 \times \frac{1}{2}(\mathrm{H}^2\mathrm{p}^2+\mathrm{H}^2\overline{\mathrm{p}}^2)$ (for **40**) and $2 \times \frac{1}{2}(\mathrm{H}^2\mathrm{p}^2+\mathrm{H}^2\overline{\mathrm{p}}^2)$ (for **41**).

[8] When we place $\mathrm{p} = \overline{\mathrm{p}}$, the term $\frac{1}{2}(\mathrm{H}^2\mathrm{p}^2+\mathrm{H}^2\overline{\mathrm{p}}^2)$ is equal to $\mathrm{H}^2\mathrm{p}^2$ (or $\mathrm{H}^2\overline{\mathrm{p}}^2$).

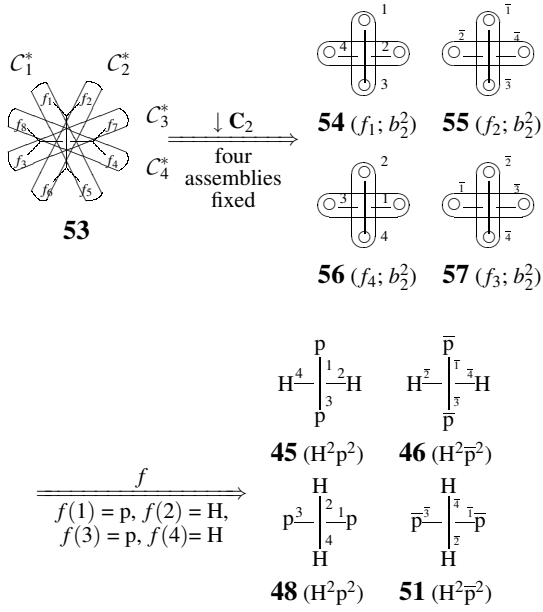

Figure 11: $\mathbf{C}_2$-Molecules (**45**, **46**, **48**, and **51**) on the reduced mandala with $\mathbf{C}_2$-assemblage (**53**). The intermediate transformulas (**54**–**57**) are selected as fixed (abstract) points in accord with the mark (= 4) for the subduction $\mathbf{D}_{2d}(/\mathbf{C}_2) \downarrow \mathbf{C}_2 = 4\mathbf{C}_2(/\mathbf{C}_2)$, which is concerned with the reduced mandala (**53**). On the other hand, each of the transformulas (**54**–**57**) shows the mode of substitution in a molecule, which is a diagrammatical expression of the subduction represented by $\mathbf{D}_{2d}(/\mathbf{C}_s) \downarrow \mathbf{C}_2 = 2\mathbf{C}_2(/\mathbf{C}_1)$.

a $\mathbf{D}_2$-molecule, which appears at the intersection of the $\mathbf{C}_2$-column and the $\mathbf{D}_{2d}(/\mathbf{D}_2)$-row of Table 1. The term $2H^2X^2$, is concerned with the mark (2) for a $\mathbf{C}_{2v}$-molecule, which appears at the intersection of the $\mathbf{C}_2$-column and the $\mathbf{D}_{2d}(/\mathbf{C}_{2v})$-row of Table 1. The term $2p^2\overline{p}^2$ is concerned with the mark (2) for an $\mathbf{S}_4$-molecule, which appears at the intersection of the $\mathbf{C}_2$-column and the $\mathbf{D}_{2d}(/\mathbf{S}_4)$-row of Table 1. Thus, Theorem 1 holds true, because the groups $\mathbf{D}_{2d}$, $\mathbf{D}_2$, $\mathbf{C}_{2v}$, and $\mathbf{S}_4$ are the supergroups of $\mathbf{C}_2$. Note that respective pairs of enantiomers are taken into consideration in the evaluation of marks.

The remaining terms appearing in eq. 7 are concerned with $\mathbf{C}_2$-molecules, each of which corresponds to the coefficient of the term at issue. Thus, the mark (4) appearing at the intersection of the $\mathbf{D}_{2d}(/\mathbf{C}_2)$-row and the $\downarrow \mathbf{C}_2$-column (Table 1) can be correlated to the coefficients of these terms: $4 \times \frac{1}{2}(H^2p^2 + H^2\overline{p}^2)$ (the mark 4 for **45/46/48/51**) and $4 \times \frac{1}{2}(X^2p^2 + X^2\overline{p}^2)$ (**45** etc. in which the two H's are replaced by two X's).

2.2.5 C_{2v}-Molecules

Row View for C_{2v}-Molecules. The action of a function f (i.e., $f(1) = \mathrm{X}$, $f(2) = \mathrm{H}$, $f(3) = \mathrm{X}$, and $f(4) = \mathrm{H}$) generates a di-X-substituted allene derivative of $\mathbf{C}_{2v}$-symmetry (**58**), as shown in Fig. 12. The corresponding reduced mandala (Fig. 12) is generated by the symmetry operations of $\mathbf{D}_{2d}$, which transform **58** (f_1) into the transformulas (**58**–**65**, i.e., f_1–f_8). As found easily, the reduced mandala (Fig. 12) is spontaneously assembled to give two assemblies, $\{f_1, f_2, f_5, f_6\}$ (**58/59/62/63**) and $\{f_7, f_4, f_3, f_8\}$ (**60/61/64/65**), each of which represents a $\mathbf{C}_{2v}$-molecule permuted under $\mathbf{D}_{2d}$.

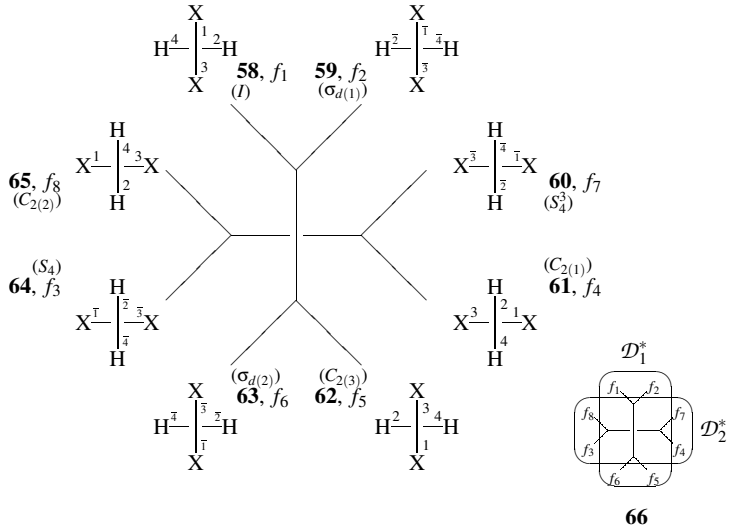

Figure 12: Reduced mandala with $\mathbf{C}_{2v}$-transformulas derived from an allene skeleton, the vertices of which construct an orbit governed by the subduction of the CR $\mathbf{D}_{2d}(/\mathbf{C}_s) \downarrow \mathbf{C}_{2v} = \mathbf{C}_{2v}(/\mathbf{C}_s) + \mathbf{C}_{2v}(/\mathbf{C}'_s)$. The $\mathbf{C}_{2v}$-transformulas are assembled into two assemblies (**58/59/62/63** and **60/61/64/65**), which construct a two-membered orbit governed by the CR $\mathbf{D}_{2d}(/\mathbf{C}_{2v})$. The orbit (representing a di-X-allene molecule) is characterized by marks $(2,2,0,2,0,2,0,0)$.

A simplified reduced mandala (**66**) is obtained by placing $\mathcal{D}_1^* = \{f_1, f_2, f_5, f_6\}$ (**58/59/62/63**) and $\mathcal{D}_2^* = \{f_7, f_4, f_3, f_8\}$ (**60/61/64/65**) in the reduced mandala shown in Fig. 12. Thereby, there emerges a two-membered $\mathbf{D}_{2d}(/\mathbf{C}_{2v})$-orbit, i.e., $\mathcal{D}^* = \{\mathcal{D}_1^*, \mathcal{D}_2^*\}$. The orbit $\mathcal{D}^*$ can be characterized by the fixation of the simplified reduced mandala (**66**) by each subgroup of $\mathbf{D}_{2d}$. The number (mark) of fixed assemblies among $\mathcal{D}_1^*$ and $\mathcal{D}_2^*$ is evaluated diagrammatically, as has been already discussed in Part 2. Thereby, an FPV $(2,2,0,2,0,2,0,0)$ is obtained by aligning the resulting numbers (marks) in the order of the SSG (eq. 1).

The fixation process for obtaining the FPV corresponds to the subduction $\mathbf{D}_{2d}(/\mathbf{C}_{2v}) \downarrow \mathbf{H}$, where the subgroup $\mathbf{H}$ is selected from the SSG (eq. 1). For example, the subduction $\mathbf{D}_{2d}(/\mathbf{C}_{2v}) \downarrow \mathbf{C}_{2v}$ causes the fixation of the two-membered $\mathbf{D}_{2d}(/\mathbf{C}_{2v})$-orbit ($\mathcal{D}^*$) in the simplified reduced mandala (**66**). Thereby, the orbit $\mathcal{D}^*$ is restricted within $\mathbf{C}_{2v}$ so as to be divided

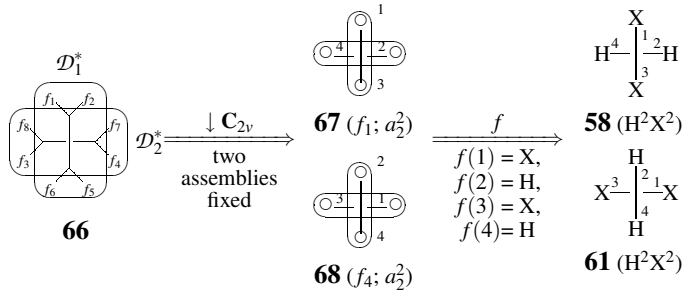

Figure 13: $\mathbf{C}_{2v}$-Molecules (**58** and **61**) on the reduced mandala with $\mathbf{C}_{2v}$-assemblage (**66**). The intermediate transformulas (**67** and **68**) are selected as fixed (abstract) points in accord with the mark (= 2) for the subduction $\mathbf{D}_{2d}(/\mathbf{C}_{2v}) \downarrow \mathbf{C}_{2v} = 2\mathbf{C}_{2v}(/\mathbf{C}_{2v})$, which is concerned with the reduced mandala (**66**). On the other hand, each of the transformulas (**67** and **68**) shows the mode of substitution in a molecule, which is a diagrammatical expression of the subduction represented by $\mathbf{D}_{2d}(/\mathbf{C}_s) \downarrow \mathbf{C}_{2v} = \mathbf{C}_{2v}(/\mathbf{C}_s) + \mathbf{C}_{2v}(/\mathbf{C}_s')$.

into two one-membered suborbits, i.e., $\{\mathcal{D}_1^*\}$ and $\{\mathcal{D}_2^*\}$. Hence, the corresponding mark is determined to be equal to 2, which appears as the sixth element of the FPV $(2,2,0,2,0,2,0,0)$. This fact is designated by the symbol $2H^2X^2$.

Fixation and $\mathbf{C}_{2v}$-Molecules. In order that the data described above are applied to chemical combinatorics, it is informative to use a diagram for the systematic explanation of the fixation process (Fig. 13). According to the subduction $\mathbf{D}_{2d}(/\mathbf{C}_{2v}) \downarrow \mathbf{C}_{2v}$ for the reduced mandala **66**), both the assemblies $\mathcal{D}_1^*$ and $\mathcal{D}_2^*$ of the orbit $\mathcal{D}^*$ are fixed to give transformulas **67** and **68** as representatives in Fig. 13. Because the four vertices (substitution positions) of each transformula originally construct an $\mathbf{D}_{2d}(/\mathbf{C}_s)$-orbit, the fixation (desymmetrization) causes the subduction $\mathbf{D}_{2d}(/\mathbf{C}_s) \downarrow \mathbf{C}_{2v}$. As a result, the original CR $\mathbf{D}_{2d}(/\mathbf{C}_s)$ for allene suffers from the subduction represented by $\mathbf{D}_{2d}(/\mathbf{C}_s) \downarrow \mathbf{C}_{2v} = \mathbf{C}_{2v}(/\mathbf{C}_s) + \mathbf{C}_{2v}(/\mathbf{C}_s')$ (cf. Part 1). Thus, the orbit of the four substitution positions (vertices) is divided into two suborbits, i.e., $\{1,3\}$ and $\{2,4\}$, as shown in **67** and **68**. Because each two-membered orbit $\mathbf{C}_{2v}(/\mathbf{C}_s)$ is homospheric (the sphericity index: a_2 for positions $\{1,3\}$ or positions $\{2,4\}$), we can obtain a_2^2 as the corresponding USCI-CF. The chirality fittingness due to each sphericity index appearing in the USCI-CF (Table 2 of Part 1) permits the accommodation represented by the function f, i.e., $f(1) = \mathrm{X}$, $f(2) = \mathrm{H}$, $f(3) = \mathrm{X}$, and $f(4) = \mathrm{H}$. As a result, **67** and **68** are respectively converted into **58** and **61**. These are equivalent under $\mathbf{D}_{2d}$ but counted distinctly as two fixed molecules (assemblies), so that the mark for $\mathbf{D}_{2d}(/\mathbf{C}_{2v}) \downarrow \mathbf{C}_{2v}$ is determined to be 2.

As found easily, the transformulas **67** and **68** exhibit the same division of vertices without taking the modes of numbering into consideration. Hence, The treatment described for Fig. 13 can be alternatively discussed by using either one of the transformulas **67** and **68**. Thus, **58** and **61** are alternatively obtained by selecting **67** and by using different functions, f and f', where we place f: $f(1) = \mathrm{X}$, $f(2) = \mathrm{H}$, $f(3) = \mathrm{X}$, and $f(4) = \mathrm{H}$; and f': $f'(1) = \mathrm{H}$, $f'(2) = \mathrm{X}$, $f'(3) = \mathrm{H}$, and $f'(4) = \mathrm{X}$.

Even if four substituents are selected from achiral ligands (H and X) and a pair of enan-

tiomeric chiral ligands (p and $\overline{\mathrm{p}}$), the chirality fittingness due to the homosphericity of the two suborbits ($\{1,3\}$ and $\{2,4\}$) permits them to accommodate achiral ligands (H and X) only (cf. Table 2 of Part 1 by keeping the USCI-CF (a_2^2) in mind). This means that the one case shown in Fig. 13 is permissible.

Column View for $\mathbf{C}_{2v}$-Molecules. Each two-membered homospheric orbit (a_2 appearing in a_2^2) can accommodate two achiral ligands of the same kind (H or X) even if chiral ligands (p and $\overline{\mathrm{p}}$) are taken into consideration. Hence, the following ligand inventory is used to evaluate marks of the $\downarrow \mathbf{C}_{2v}$-column.

$$a_2 = \mathrm{H}^2 + \mathrm{X}^2 \tag{8}$$

It follows that the following generating function is obtained to evaluate marks of the $\downarrow \mathbf{C}_{2v}$-column:

$$\begin{aligned} a_2^2 &= (\mathrm{H}^2 + \mathrm{X}^2)^2 \\ &= (\mathrm{H}^4 + \mathrm{X}^4) + 2\mathrm{H}^2\mathrm{X}^2 \end{aligned} \tag{9}$$

Among the terms appearing in eq. 9, the term H^4 (or X^4) is concerned with the mark (1) for a $\mathbf{D}_{2d}$-molecule, which appears at the intersection of the $\mathbf{C}_{2v}$-column and the $\mathbf{D}_{2d}(/\mathbf{D}_{2d})$-row of the mark table (Table 1). Theorem 1 holds true, because the group $\mathbf{D}_{2d}$ is the supergroup of $\mathbf{C}_{2v}$.

The remaining term appearing in eq. 9 is concerned with a $\mathbf{C}_{2v}$-molecule, which corresponds to the coefficient of the term at issue. Thus, the mark (2) appearing at the intersection of the $\mathbf{D}_{2d}(/\mathbf{C}_{2v})$-row and the $\downarrow \mathbf{C}_{2v}$-column (Table 1) can be correlated to the coefficients of the term $2\mathrm{H}^2\mathrm{X}^2$ (**58/61**).

2.2.6 Molecules of Other Symmetries

Row View for Molecules of Other Symmetries. Molecules corresponding to the remaining subgroups of $\mathbf{D}_{2d}$ can be studied similarly. Their derivation is open to the challenge of readers as follows:

Exercise 1. Show $\mathbf{D}_2$-molecules by considering the corresponding mandala. See Fig. 3 of Part 1 as an example of $\mathbf{D}_2$-molecule.

Exercise 2. Show $\mathbf{S}_4$-molecules by considering the corresponding mandala. See Fig. 3 of Part 1 as an example of $\mathbf{S}_4$-molecule.

Exercise 3. Show $\mathbf{C}_1$-molecules by considering the corresponding mandala. See Fig. 3 of Part 1 as an example of $\mathbf{C}_1$-molecule.

Column View for Molecules of Other Symmetries. Because the USCI-CF for $\mathbf{D}_{2d}(/\mathbf{C}_s) \downarrow \mathbf{D}_2$ is b_4 (cf. Table 1), the corresponding ligand inventory is found to be:

$$b_4 = \mathrm{H}^4 + \mathrm{X}^4 + \mathrm{p}^4 + \overline{\mathrm{p}}^4, \tag{10}$$

which is equal to the generating function of this case but is transformed as follows to show relevant marks:

$$b_4 = (\mathrm{H}^4 + \mathrm{X}^4) + 2 \times \frac{1}{2}(\mathrm{p}^4 + \overline{\mathrm{p}}^4), \tag{11}$$

Obviously, the term H^4 (or X^4) in eq. 11 represents the mark (1) for a $\mathbf{D}_{2d}$-molecule, because the $\mathbf{D}_{2d}$ is a supergroup of the $\mathbf{D}_2$. The remaining terms are regarded as a combined term, i.e., $2 \times \frac{1}{2}(p^4 + \overline{p}^4)$, which represents the mark (2) for a $\mathbf{D}_2$-molecule. These marks appear in the $\downarrow \mathbf{D}_2$-column of Table 1.

Because the USCI-CF for $\mathbf{D}_{2d}(/\mathbf{C}_s) \downarrow \mathbf{S}_4$ is c_4 (cf. Table 1), the corresponding ligand inventory is found to be:

$$c_4 = H^4 + X^4 + 2p^2\overline{p}^2 \tag{12}$$

which is equal to the generating function of this case. Note that the term $2p^2\overline{p}^2$ is regarded as representing a pairwise packing of the $\mathbf{S}_4(/\mathbf{C}_1)$-orbit (USCI-CF c_4) when eq. 12 is regarded as a ligand inventory. At the same time, the coefficient of the same term is regarded as representing the mark 2 for an $\mathbf{S}_4$-molecule of the molecular formula $p^2\overline{p}^2$, when eq. 12 is regarded as a generating function. The term H^4 (orX^4) in eq. 12 (as a generating function) represents the mark (1) for a $\mathbf{D}_{2d}$-molecule, because the $\mathbf{D}_{2d}$ is a supergroup of the $\mathbf{S}_4$.

As for $\downarrow \mathbf{C}_1$, the sphericity index b_1 in the USCI-CF (b_1^4) shown in Table 1 is substituted by the following ligand inventory:

$$b_1 = H + X + p + \overline{p} \tag{13}$$

Thereby, the generating function for $\downarrow \mathbf{C}_1$ is calculated to be:

$$\begin{aligned}
b_1^4 &= (H+X+p+\overline{p})^4 \\
&= (H^4+X^4)+(4H^3X+4HX^3)+6H^2X^2 \\
&\quad +8\times\frac{1}{2}(H^3p+H^3\overline{p})+8\times\frac{1}{2}(X^3p+X^3\overline{p})+ \\
&\quad +24\times\frac{1}{2}(H^2Xp+H^2X\overline{p})+24\times\frac{1}{2}(HX^2p+HX^2\overline{p})+ \\
&\quad +12\times\frac{1}{2}(H^2p^2+H^2\overline{p}^2)+12\times\frac{1}{2}(X^2p^2+X^2\overline{p}^2)+24\times\frac{1}{2}(HXp^2+HX\overline{p}^2) \\
&\quad +(12H^2p\overline{p}+12X^2p\overline{p})+24HXp\overline{p} \\
&\quad +24\times\frac{1}{2}(Hp^2\overline{p}+Hp\overline{p}^2)+24\times\frac{1}{2}(Xp^2\overline{p}+Xp\overline{p}^2) \\
&\quad +8\times\frac{1}{2}(Hp^3+H\overline{p}^3)+8\times\frac{1}{2}(Xp^3+X\overline{p}^3) \\
&\quad +6p^2\overline{p}^2+8\times\frac{1}{2}(p^3\overline{p}+p\overline{p}^3)+2\times\frac{1}{2}(p^4+\overline{p}^4)
\end{aligned} \tag{14}$$

3 Combinatorial Enumeration

3.1 Linking Row Views with Column Views

As found in the preceding section, the column view for each symmetry ($\downarrow \mathbf{H}$) has given a generating function, in which the coefficient of the term $H^{x_1}X^{x_2}p^{x_3}\overline{p}^{x_4}$ (or the combined one) represents the mark for $\mathbf{H}$-molecules having the formula $H^{x_1}X^{x_2}p^{x_3}\overline{p}^{x_4}$. Hence, such marks are collected with respect to the symmetry $\mathbf{H}$ (as columns), giving Table 2. For example, the coefficients of the terms in eq. 5 appear in the $\downarrow \mathbf{C}_s$-column of Table 2. Tables of this type are regarded as matrices and called *fixed-point matrices* (FPMs). The correspondence between each column and the generating function at issue is shown in the top part of Table 2. Note that each combined

Table 2: FPVs Appearing in an FPM Calculated by Generating Functions Based on Column Views

USCI-CFs for Positions of a $\mathbf{D}_{2d}$-Skeleton

$\mathbf{D}_{2d}(/\mathbf{C}_s)$	b_1^4	b_2^2	b_2^2	$a_1^2c_2$	c_4	a_2^2	b_4	a_4
	↕	↕	↕	↕	↕	↕	↕	↕
Generating Functions for FPVs								
	eq. 14	eq. 7	eq. 7	eq. 5	eq. 12	eq. 9	eq. 11	eq. 2
	↕	↕	↕	↕	↕	↕	↕	↕

FPVs for Counting Stereoisomers: FPM

formula[a]	$\downarrow\mathbf{C}_1$	$\downarrow\mathbf{C}_2$	$\downarrow\mathbf{C}_2^{'}$	$\downarrow\mathbf{C}_s$	$\downarrow\mathbf{S}_4$	$\downarrow\mathbf{C}_{2v}$	$\downarrow\mathbf{D}_2$	$\downarrow\mathbf{D}_{2d}$
H^4, X^4	1	1	1	1	1	1	1	1
H^3X, HX^3	4	0	0	2	0	0	0	0
H^2X^2	6	2	2	2	0	2	0	0
H^3p, X^3p	8	0	0	0	0	0	0	0
H^2Xp, HX^2p	24	0	0	0	0	0	0	0
H^2p^2, X^2p^2	12	4	4	0	0	0	0	0
$H^2p\overline{p}$, $X^2p\overline{p}$	12	0	0	2	0	0	0	0
HXp^2	24	0	0	0	0	0	0	0
$HXp\overline{p}$	24	0	0	4	0	0	0	0
$Hp^2\overline{p}$, $Xp^2\overline{p}$	24	0	0	0	0	0	0	0
Hp^3, Xp^3	8	0	0	0	0	0	0	0
$p^2\overline{p}^2$	6	2	2	0	2	0	0	0
$p^3\overline{p}$	8	0	0	0	0	0	0	0
p^4	2	2	2	0	0	0	2	0

[a]Each combined term is designated by a representative term to save spaces.

term for a pair of enantiomers (e.g., $\frac{1}{2}(p^4+\overline{p}^4)$) is designated by a representative term (e.g., p^4) for the sake of space saving.

The same FPM (Table 2) can be alternatively examined in terms of the row view, in which each row is regarded as the FPV concerning the formula $H^{x_1}X^{x_2}p^{x_3}\overline{p}^{x_4}$. There are several simple cases in explaining the FPVs collected in Table 2. For example, the FPV $(1,1,1,1,1,1,1,1)$ for the H^4-row (or X^4-row) is identical with the $\mathbf{D}_{2d}(/\mathbf{D}_{2d})$-row of Table 1. This means that the H^4-row (or X^4-row) corresponds to one $\mathbf{D}_{2d}$-stereoisomer in terms of the reduced mandala shown in Fig. 2. The [H^4,$\mathbf{D}_{2d}$]-stereoisomer (**2**) and the [X^4,$\mathbf{D}_{2d}$]-stereoisomer (**12**) are shown in Fig. 3.[9]

The FPV $(4,0,0,2,0,0,0,0)$ for the H^3X-row (or HX^3-row) is identical with the $\mathbf{D}_{2d}(/\mathbf{C}_s)$-row of Table 1 so that the H^3X-row (or HX^3-row) corresponds to one $\mathbf{C}_s$-stereoisomer in

[9]The term "[H^4,$\mathbf{D}_{2d}$]-stereoisomer" is used to designate a stereoisomer with the formula H^4 and the $\mathbf{D}_{2d}$-symmetry.

terms of the mandala shown in Fig. 4. The [H^3X,$\mathbf{C}_s$]-stereoisomer (**13**) and the [HX^3,$\mathbf{C}_s$]-stereoisomer (**26**) are shown in Fig. 6.

The FPV $(2,2,2,0,0,0,2,0)$ for the p^4-row is identical with the $\mathbf{D}_{2d}(/\mathbf{D}_2)$-row of Table 1. Hence, the p^4-row corresponds to one $\mathbf{D}_2$-stereoisomer.

Exercise 4. Show the [p^4,$\mathbf{D}_2$]-stereoisomer.

Similarly, the presence of one $\mathbf{C}_1$-stereoisomer (as a pair of enantiomers) is shown by the FPV $(8,0,0,0,0,0,0,0)$ for the H^3p-row (or X^3p-row), the Hp^3-row (or Xp^3-row), or the $p^3\overline{p}$-row.

Exercise 5. Show the [H^3p,$\mathbf{C}_1$]-stereoisomer, the [X^3p,$\mathbf{C}_1$]-stereoisomer, the [Hp^3,$\mathbf{C}_1$]-stereoisomer, the [Xp^3,$\mathbf{C}_1$]-stereoisomer, and the [$p^3\overline{p}$,$\mathbf{C}_1$]-stereoisomer.

The remaining FPVs appearing in Table 2 can be explained by an appropriate summation of $\mathbf{D}_{2d}(/\mathbf{H})$-rows of the mark table (Table 1). For example, the FPV $(6,2,2,2,0,2,0,0)$ for the H^2X^2-row of Table 2 is explained as follows:

$\mathbf{D}_{2d}(/\mathbf{C}_2')$	4	0	2	0	0	0	0	0	
$\mathbf{D}_{2d}(/\mathbf{C}_{2v})$	2	2	0	2	0	2	0	0	(+
	6	2	2	2	0	2	0	0	

where the data of the $\mathbf{D}_{2d}(/\mathbf{C}_2')$-row and the $\mathbf{D}_{2d}(/\mathbf{C}_{2v})$-row listed in Table 1 are summed up. It follows that there exist one $\mathbf{C}_2'$-stereoisomer with the term H^2X^2 and one $\mathbf{C}_{2v}$-stereoisomer with the term H^2X^2. They are depicted in Fig. 8 (**29**) and Fig. 13 (**58**). The corresponding reduced mandalas are shown in Figs. 7 and 12.

The FPV $(6,2,2,0,2,0,0,0)$ for the $p^2\overline{p}^2$-row of Table 2 is explained as follows:

$\mathbf{D}_{2d}(/\mathbf{C}_2')$	4	0	2	0	0	0	0	0	
$\mathbf{D}_{2d}(/\mathbf{S}_4)$	2	2	0	0	2	0	0	0	(+
	6	2	2	0	2	0	0	0	

where the data of the $\mathbf{D}_{2d}(/\mathbf{C}_2')$-row and the $\mathbf{D}_{2d}(/\mathbf{S}_4)$-row listed in Table 1 are summed up. It follows that there exist one $\mathbf{C}_2'$-stereoisomer with the term $p^2\overline{p}^2$ and one $\mathbf{S}_4$-stereoisomer with the term $p^2\overline{p}^2$. The [$p^2\overline{p}^2$,$\mathbf{C}_2'$]-stereoisomer is depicted Fig. 10 (**45**).

Exercise 6. Depict the [$p^2\overline{p}^2$,$\mathbf{S}_4$]-stereoisomer. Compare this with the [$p^2\overline{p}^2$,$\mathbf{C}_2'$]-stereoisomer (**45**).

Exercise 7. Show that the FPV for H^2Xp-row of Table 2 is calculated by three times of the $\mathbf{D}_{2d}(/\mathbf{C}_1)$-row of Table 1. Examine also HXp^2-row and $Hp^2\overline{p}$-row.

Exercise 8. Show that the FPV for H^2p^2-row of Table 2 is calculated by the summation of the $\mathbf{D}_{2d}(/\mathbf{C}_2)$-row and the $\mathbf{D}_{2d}(/\mathbf{C}_2')$-row (two times) of Table 1. See Figs. 9 and 11.

Exercise 9. Show that the FPV for $H^2p\overline{p}$-row of Table 2 is calculated by the summation of the $\mathbf{D}_{2d}(/\mathbf{C}_1)$-row and the $\mathbf{D}_{2d}(/\mathbf{C}_s)$-row of Table 1.

Exercise 10. Show that the FPV for $HXp\overline{p}$-row of Table 2 is calculated by the summation of the $\mathbf{D}_{2d}(/\mathbf{C}_1)$-row (two times) and the $\mathbf{D}_{2d}(/\mathbf{C}_s)$-row (two times) of Table 1.

3.2 Fixed-Point Matrices and Isomer-Counting Matrices

As found in Subsection 3.1, the linking of row views with column views has provided us with a tool for enumerating stereoisomers, although the final results of stereoisomer numbers have been obtained by somewhat try-and-error calculations. In order to generalize the linking procedure, however, a more algebraic approach is necessary.

Let us consider the FPV $(6,2,2,2,0,2,0,0)$ for the H^2X^2-row of Table 2, which has been concluded to be equal to the summation of the marks for $\mathbf{D}_{2d}(/\mathbf{C}_2')$ and $\mathbf{D}_{2d}(/\mathbf{C}_{2v})$ by the try-and-error calculation (Subsection 3.1). The latter result is represented by an isomer-counting vector (ICV): $(0,0,1,0,0,1,0,0)$, in which the numbers of **H**-stereoisomers are aligned in the order of **H** appearing in the SSG (eq. 1). When the mark table (Table 1) is regarded as a square matrix ($M_{\mathbf{D}_{2d}}$), the conversion of the FPV into the ICV is represented by the following equation:

$$(6,2,2,2,0,2,0,0) = (0,0,1,0,0,1,0,0)M_{\mathbf{D}_{2d}}. \tag{15}$$

Obviously, this equation means that the $\mathbf{D}_{2d}(/\mathbf{C}_2')$-row and the $\mathbf{D}_{2d}(/\mathbf{C}_{2v})$-row of Table 1 are summed up (the right-hand side) so as to give the FPV (the left-hand side) in agreement with the result described in Subsection 3.1. Because the $M_{\mathbf{D}_{2d}}$ is a lower-triangular matrix with non-zero diagonal elements, it has the inverse matrix ($M^{-1}_{\mathbf{D}_{2d}}$). Thereby, the ICV can be obtained from the FPV by means of the following equation:

$$(0,0,1,0,0,1,0,0) = (6,2,2,2,0,2,0,0)M^{-1}_{\mathbf{D}_{2d}}, \tag{16}$$

where we place

$$M^{-1}_{\mathbf{D}_{2d}} = \begin{pmatrix} \frac{1}{8} & 0 & 0 & 0 & 0 & 0 & 0 & 0 \\ -\frac{1}{8} & \frac{1}{4} & 0 & 0 & 0 & 0 & 0 & 0 \\ -\frac{1}{4} & 0 & \frac{1}{2} & 0 & 0 & 0 & 0 & 0 \\ -\frac{1}{4} & 0 & 0 & \frac{1}{2} & 0 & 0 & 0 & 0 \\ 0 & -\frac{1}{4} & 0 & 0 & \frac{1}{2} & 0 & 0 & 0 \\ \frac{1}{4} & -\frac{1}{4} & 0 & -\frac{1}{2} & 0 & \frac{1}{2} & 0 & 0 \\ \frac{1}{4} & -\frac{1}{4} & -\frac{1}{2} & 0 & 0 & 0 & \frac{1}{2} & 0 \\ 0 & \frac{1}{2} & 0 & 0 & -\frac{1}{2} & -\frac{1}{2} & -\frac{1}{2} & 1 \end{pmatrix} \begin{matrix} \frac{1}{8} \\ \frac{1}{8} \\ \frac{1}{4} \\ \frac{1}{4} \\ \frac{1}{4} \\ 0 \\ 0 \\ 0 \end{matrix}. \tag{17}$$

On the same line as eq. 16, each row of Table 2 is multiplied by the inverse ($M^{-1}_{\mathbf{D}_{2d}}$) to give the corresponding ICV. Such ICVs are collected to give Table 3, which can be regarded as a matrix called *an isomer-counting matrix* (ICM). Examples of molecules for each column are shown in the bottom row of Table 3, where the vacant examples should be filled by means of Exercises 1–3.

When Table 2 is regarded as a matrix called *a fixed-point matrix* (FPM), the above results, i.e., the conversions between Table 2 (FPM) and Table 3 (ICM), are represented by the following equations:

$$\mathrm{FPM} = \mathrm{ICM} \times M_{\mathbf{D}_{2d}} \tag{18}$$

and

$$\mathrm{ICM} = \mathrm{FPM} \times M^{-1}_{\mathbf{D}_{2d}} \tag{19}$$

Table 3: Numbers of Stereoisomers with Itemized Formulas and Symmetries (ICM)

formula[a]	$\downarrow\mathbf{C}_1$	$\downarrow\mathbf{C}_2$	$\downarrow\mathbf{C}_2'$	$\downarrow\mathbf{C}_s$	$\downarrow\mathbf{S}_4$	$\downarrow\mathbf{C}_{2v}$	$\downarrow\mathbf{D}_2$	$\downarrow\mathbf{D}_{2d}$	
H^4, X^4	0	0	0	0	0	0	0	1	1
H^3X, HX^3	0	0	0	1	0	0	0	0	1
H^2X^2	0	0	1	0	0	1	0	0	2
H^3p, X^3p	1	0	0	0	0	0	0	0	1
H^2Xp, HX^2p	3	0	0	0	0	0	0	0	3
H^2p^2, X^2p^2	0	1	2	0	0	0	0	0	3
$H^2p\overline{p}$, $X^2p\overline{p}$	1	0	0	1	0	0	0	0	2
HXp^2	3	0	0	0	0	0	0	0	3
$HXp\overline{p}$	2	0	0	2	0	0	0	0	4
$Hp^2\overline{p}$, $Xp^2\overline{p}$	3	0	0	0	0	0	0	0	3
Hp^3, Xp^3	1	0	0	0	0	0	0	0	1
$p^2\overline{p}^2$	0	0	1	0	1	0	0	0	2
$p^3\overline{p}$	1	0	0	0	0	0	0	0	1
p^4	0	0	0	0	0	0	1	0	1
Examples		**45**	Fig. 9	Fig. 6		**58**		Fig. 3	

[a]Each combined term is designated by a representative term to save spaces.

3.3 Formulation of Stereoisomer Counting

The diagrammatical discussions described above can be generalized easily to give versatile theorems, which are essentially equivalent to Theorem 19.4 and Lemma 19.2 proved more mathematically in Chapter 19 of Fujita's book [6]. The original mathematical versions of the proofs have appeared in a previous paper [10]. Related theorems based on USCIs in place of USCI-CFs have appeared in Ref. [11] and in Chapter 15 of Fujita's book [6].

3.3.1 Generalization of FPMs and ICMs

The FPM (Table 2) and the ICM (Table 3) for enumerating allene derivatives with the formulas $H^{x_1}X^{x_2}p^{x_3}\overline{p}^{x_4}$ derived from an allene skeleton of $\mathbf{D}_{2d}$-symmetry can be generalized to accomplish the counting of stereoisomers with the weights W_θ derived from a skeleton of $\mathbf{G}$-symmetry.

Let us consider a skeleton of $\mathbf{G}$-symmetry, which is characterized by the following SSG:

$$\mathrm{SSG}_{\mathbf{G}} = \{\mathbf{G}_1(=\mathbf{C}_1), \mathbf{G}_2, \ldots, \mathbf{G}_j, \ldots, \mathbf{G}_s(=\mathbf{G})\}, \tag{20}$$

Thus, eq. 18 is generalized as follows by placing FPM ($(\rho_{\theta j})$), ICM ($(B_{\theta j})$), and the mark table

of $\mathbf{G}$ ($M_{\mathbf{G}} = (m_{ij})$):

$$\begin{pmatrix} \rho_{11} & \cdots & \rho_{1j} & \cdots & \rho_{1s} \\ \rho_{21} & \cdots & \rho_{2j} & \cdots & \rho_{2s} \\ \vdots & & \vdots & & \vdots \\ \rho_{\theta 1} & \cdots & \rho_{\theta j} & \cdots & \rho_{\theta s} \\ \vdots & & \vdots & & \vdots \\ \rho_{|\theta|1} & \cdots & \rho_{|\theta|j} & \cdots & \rho_{|\theta|s} \end{pmatrix} = \begin{pmatrix} B_{11} & \cdots & B_{1i} & \cdots & B_{1s} \\ B_{21} & \cdots & B_{2i} & \cdots & B_{2s} \\ \vdots & & \vdots & & \vdots \\ B_{\theta 1} & \cdots & B_{\theta i} & \cdots & B_{\theta s} \\ \vdots & & \vdots & & \vdots \\ B_{|\theta|1} & \cdots & B_{|\theta|i} & \cdots & B_{|\theta|s} \end{pmatrix} \begin{pmatrix} m_{11} & \cdots & m_{1j} & \cdots & m_{1s} \\ \vdots & & \vdots & & \vdots \\ m_{i1} & \cdots & m_{ij} & \cdots & m_{is} \\ \vdots & & \vdots & & \\ m_{s1} & \cdots & m_{sj} & \cdots & m_{ss} \end{pmatrix} \tag{21}$$

FPM ICM Mark Table ($M_{\mathbf{G}}$)

Hence, eq. 19 is generalized as follows by placing the inverse mark table of $\mathbf{G}$ ($M_{\mathbf{G}}^{-1} = (\overline{m}_{ij})$):

$$\begin{pmatrix} B_{11} & \cdots & B_{1i} & \cdots & B_{1s} \\ B_{21} & \cdots & B_{2i} & \cdots & B_{2s} \\ \vdots & & \vdots & & \vdots \\ B_{\theta 1} & \cdots & B_{\theta i} & \cdots & B_{\theta s} \\ \vdots & & \vdots & & \vdots \\ B_{|\theta|1} & \cdots & B_{|\theta|i} & \cdots & B_{|\theta|s} \end{pmatrix} = \begin{pmatrix} \rho_{11} & \cdots & \rho_{1j} & \cdots & \rho_{1s} \\ \rho_{21} & \cdots & \rho_{2j} & \cdots & \rho_{2s} \\ \vdots & & \vdots & & \vdots \\ \rho_{\theta 1} & \cdots & \rho_{\theta j} & \cdots & \rho_{\theta s} \\ \vdots & & \vdots & & \vdots \\ \rho_{|\theta|1} & \cdots & \rho_{|\theta|j} & \cdots & \rho_{|\theta|s} \end{pmatrix} \begin{pmatrix} \overline{m}_{11} & \cdots & \overline{m}_{i1} & \cdots & \overline{m}_{s1} \\ \vdots & & \vdots & & \vdots \\ \overline{m}_{1j} & \cdots & \overline{m}_{ij} & \cdots & \overline{m}_{sj} \\ \vdots & & \vdots & & \\ \overline{m}_{1s} & \cdots & \overline{m}_{is} & \cdots & \overline{m}_{ss} \end{pmatrix} \tag{22}$$

ICM FPM Inverse Mark Table ($M_{\mathbf{G}}^{-1}$)

Note that the value $\rho_{\theta j}$ in the FPM represents the mark of $\mathbf{G}_j$ and the weight W_θ (molecular formula) and that $B_{\theta j}$ in the ICM represents the number of stereoisomers with $\mathbf{G}_j$ and the weight W_θ (molecular formula).

In terms of the row view, each row of the FPM in eqs. 21 and 22 represents an FPV $(\rho_{\theta 1}, \rho_{\theta 2}, \ldots, \rho_{\theta s})$ for determining the numbers $(B_{\theta i})$ of $[W_\theta, \mathbf{G}_i]$-stereoisomers $(i = 1, 2, \ldots, s)$. Remember that the number $B_{\theta i}$ is the multiplicity of the CR $\mathbf{G}(/\mathbf{G}_i)$ corresponding to a reduced mandala with $\mathbf{G}_i$-assemblage.

In terms of the column view, on the other hand, each column of the same FPM (eqs. 21 and 22) appears as the coefficients of a generating function derived from a subduced cycle index with chirality fittingness (SCI-CF), which is a product of such USCI-CFs as discussed below more clearly.

3.3.2 Subduced-Cycle-Index (SCI) Method for Stereoisomer Counting

The allene skeleton has one orbit governed by $\mathbf{D}_{2d}(/\mathbf{C}_s)$, where USCI-CFs have been directly used for calculating FPVs. To discuss general cases, however, a skeleton having two ore more orbits should be taken into consideration, where subduced cycle indices with chirality fittingness (SCI-CFs) are used in place of the USCI-CFs.

Suppose that an orbit ($O^{(\alpha)}$) of substitution positions of a given skeleton of $\mathbf{G}$ is governed by the CR $\mathbf{G}(/\mathbf{G}_\ell)$, where the size of the orbit $|O^{(\alpha)}|$ is equal to the degree of the CR, i.e., $|\mathbf{G}|/|\mathbf{G}_\ell|$. The orbit $O^{(\alpha)}$ accommodates achiral ligands selected from the following set:

$$\mathbf{X}^{(\alpha)} = \{\mathrm{X}_1, \mathrm{X}_2, \ldots, \mathrm{X}_x\} \tag{23}$$

as well as chiral ligands selected from the following set:

$$\mathbf{p}^{(\alpha)} = \{\mathrm{p}_1, \mathrm{p}_2, \ldots, \mathrm{p}_p; \quad \overline{\mathrm{p}}_1, \overline{\mathrm{p}}_2, \ldots, \overline{\mathrm{p}}_p\}, \tag{24}$$

where p_i and $\overline{\mathrm{p}}_i$ represent a pair of enantiomers ($i = 1, 2, \ldots, p$). When the orbit $O^{(\alpha)}$ accommodates θ_1 of $\mathrm{X}_1, \ldots, \theta_x$ of X_x; θ'_1 of $\mathrm{p}_1, \ldots, \theta'_p$ of p_p; and θ''_1 of $\overline{\mathrm{p}}_1, \ldots, \theta''_p$ of $\overline{\mathrm{p}}_p$, the corresponding weight (molecular formula) is represented by the following equation:

$$W_\theta^{(\alpha)} = \mathrm{X}_1^{\theta_1} \cdots \mathrm{X}_x^{\theta_x} \mathrm{p}_1^{\theta'_1} \cdots \mathrm{p}_p^{\theta'_p} \overline{\mathrm{p}}_1^{\theta''_1} \cdots \overline{\mathrm{p}}_p^{\theta''_p}, \tag{25}$$

where the powers satisfies the following partition:

$$[\theta]^{(\alpha)}: \quad (\theta_1 + \cdots + \theta_x) + (\theta'_1 + \cdots + \theta'_p) + (\theta''_1 + \ldots + \theta''_p) = |O^{(\alpha)}|. \tag{26}$$

The orbit $O^{(\alpha)}$ of $\mathbf{G}$-symmetry is restricted into its subgroup $\mathbf{G}_j$ in accord with the subduction represented by $\mathbf{G}(/\mathbf{G}_\ell) \downarrow \mathbf{G}_j$, which is characterized by the corresponding USCI-CF, i.e.,

$$\text{USCI-CF}(\mathbf{G}_j; a_d, b_d, c_d)^{(\alpha)}. \tag{27}$$

When the orbit $O^{(\alpha)}$ runs to cover all of the substitution positions of the skeleton (i.e., $O = \bigcup_\alpha O^{(\alpha)}$), the USCI-CF (eq. 27) gives the following product:

$$\text{SCI-CF}(\mathbf{G}_j; a_d, b_d, c_d) = \prod_\alpha \text{USCI-CF}(\mathbf{G}_j; a_d, b_d, c_d)^{(\alpha)}, \tag{28}$$

which are called *a subduced cycle index with chirality fittingness* (SCI-CF). The sets represented by eq. 23 and 24 run according to the index α for $O^{(\alpha)}$. The weight (eq. 25) and the partition (eq. 26) also run according to the index α. In particular, the total weight is represented as follows:

$$W_\theta = \prod_\alpha W_\theta^{(\alpha)}. \tag{29}$$

The column view for the FPM provides us with the following theorem:

Theorem 2. *A generating function for calculating $\rho_{\theta j}$ is obtained as follows:*

$$\sum_{[\theta]} \rho_{\theta j} W_\theta = \text{SCI-CF}(\mathbf{G}_j; a_d, b_d, c_d), \tag{30}$$

where the sphericity indices in the SCI-CF are substituted by the following ligand inventories:

$$a_d^{(\alpha)} = \mathrm{X}_1^d + \cdots + \mathrm{X}_x^d \tag{31}$$

$$c_d^{(\alpha)} = \mathrm{X}_1^d + \cdots + \mathrm{X}_x^d + 2(\mathrm{p}_1^{d/2} \overline{\mathrm{p}}_1^{d/2} + \cdots \mathrm{p}_p^{d/2} \overline{\mathrm{p}}_p^{d/2}) \tag{32}$$

$$b_d^{(\alpha)} = (\mathrm{X}_1^d + \cdots + \mathrm{X}_x^d) + (\mathrm{p}_1^d + \cdots + \mathrm{p}_p^d) + (\overline{\mathrm{p}}_1^d + \cdots + \overline{\mathrm{p}}_p^d), \tag{33}$$

where the index α of each inventory corresponds to the USCI-CFs shown in the right-hand side of eq. 28.

This theorem is equivalent to Lemma 19.2 of Fujita's book [6]. It should be noted that the ligand sets represented by eqs. 23 and 24 can be selected independently according to the properties of the orbits ($O^{(\alpha)}$).[10] Alternatively, the weights represented by (eq. 25) may be varied according to the orbits ($O^{(\alpha)}$).

[10] One of these cases is formulated as the concept of "obligatory minimum valencies", which has been discussed in Chapter 14 of Fujita's book [6].

Theorem 3 (SCI Method). *The marks $\rho_{\theta j}$ calculated by eq. 30 construct the j-th column of the FPM (eq. 22). Thereby, the ICM is obtained by using eq. 22. The resulting $B_{\theta j}$ is the number of $[W_\theta, \mathbf{G}_j]$-stereoisomers.*

This theorem is equivalent to Theorem 19.4 of Fujita's book [6]. The stereoisomer counting based on Theorems 2 and 3 is called *the SCI method*.

Exercise 11. Reexamine Tables 2 and 3 in terms of Theorems 2 and 3.

Exercise 12. Calculate the numbers of stereoisomers derived from adamantane-2,6-dione of $\mathbf{D}_{2d}$-symmetry by following the stepwise procedure:

1. Show that the 12 positions of adamantane-1,6-dione as a skeleton are characterized by an FPV $(12,0,0,2,0,0,0,0)$.

2. Then this FPV is multiplied by the inverse mark table (eq. 17) to obtain an ICV.[11]

3. In terms of the ICV, show that the FPV is equal to the sum of the $\mathbf{D}_{2d}(/\mathbf{C}_1)$-row and the $\mathbf{D}_{2d}(/\mathbf{C}_s)$-row of Table 1. Confirm that they respectively govern the eight-membered orbit of the bridge hydrogens and the four-membered orbit of the bridge-head hydrogens.

4. Obtain SCI-CFs for the respective subgroups by using the USCI-CFs listed in the top part of Table 1.

5. According to Theorem 2, calculate an FPM by using the following inventories:

$$a_d = \mathrm{H}^d + \mathrm{X}^d \tag{34}$$
$$c_d = \mathrm{H}^d + \mathrm{X}^d + 2\mathrm{p}^{d/2}\overline{\mathrm{p}}^{d/2} \tag{35}$$
$$b_d = \mathrm{H}^d + \mathrm{X}^d + \mathrm{p}^d + \overline{\mathrm{p}}^d. \tag{36}$$

6. Calculate an ICM by following Theorem 3.

For Steps 1–3, see Section 5.4 of Fujita's book [6]. The algebraic procedure represented by Steps 1–3 can be replaced by the diagrammatical procedure described in Part 1. Thus, by an inspection, the twelve positions of adamantane-2,6-dione can be divided into two orbits, i.e., an orbit of eight bridge positions and another orbit of four bridge-head positions. The assignment the CRs ($\mathbf{D}_{2d}(/\mathbf{C}_1)$ and and $\mathbf{D}_{2d}(/\mathbf{C}_s)$) can be accomplished by examining the local symmetries ($\mathbf{C}_1$ and $\mathbf{C}_s$).

It should be noted that Steps 1–3 are concerned with an application of the mark table to intramolecular stereochemistry (Part 1). Moreover, Steps 4–5 are concerned with an application of the mark table to intermolecular stereochemistry (Part 2) so that the combination of Part 1 and Part 2 results in combinatorial enumeration (Part 3).

[11] Strictly speaking, the resulting row vector indicates the numbers of the orbits of substitution positions. However, the row vector is also called *an isomer-counting vector*, for the sake of simplicity.

3.3.3 Partial-Cycle-Index (PCI) Method for Stereoisomer Counting

Theorem 2 for obtaining generating functions and Theorem 3 for matrix calculations can be combined so as to reach an integrated theorem based on generating functions.

Each column of the ICM (and the FPM) in eq. 22 can be summed up after multiplication of the corresponding weight (W_θ), because each row of the ICM (and the FPM) is independent and characterized by the W_θ. Hence, we obtain the following equation:

$$\left(\sum_{[\theta]} B_{\theta 1} W_\theta, \ldots, \sum_{[\theta]} B_{\theta i} W_\theta, \ldots, \sum_{[\theta]} B_{\theta s} W_\theta\right) = \left(\sum_{[\theta]} \rho_{\theta 1} W_\theta, \ldots, \sum_{[\theta]} \rho_{\theta j} W_\theta, \ldots, \sum_{[\theta]} \rho_{\theta s} W_\theta\right) M_{\mathbf{G}}^{-1} \tag{37}$$

The resulting summation appearing in the right-hand side of eq. 37 is regarded as a row vector, which is multiplied by the i-th column of the inverse ($M_{\mathbf{G}}^{-1}$). Thereby, we can obtain the following equation as the i-th element:

$$\sum_{[\theta]} B_{\theta i} W_\theta = \sum_{j=1}^{s} (\overline{m}_{ij} \sum_{[\theta]} \rho_{\theta j} W_\theta) \quad (\text{for } i = 1, 2, \ldots, s). \tag{38}$$

By introducing eq. 30 of Theorem 2 into eq. 38, we have a following equation:

$$\sum_{[\theta]} B_{\theta i} W_\theta = \sum_{j=1}^{s} \overline{m}_{ij} \text{SCI-CF}(\mathbf{G}_j; a_d, b_d, c_d) \quad (\text{for } i = 1, 2, \ldots, s). \tag{39}$$

Alternatively, eq. 30 (Theorem 2) is first introduced into eq. 37 to give the following equation:

$$\left(\ldots, \quad \sum_{[\theta]} B_{\theta i} W_\theta, \quad \ldots\right) = \left(\ldots, \quad \text{SCI-CF}(\mathbf{G}_j; a_d, b_d, c_d), \quad \ldots\right) M_{\mathbf{G}}^{-1} \tag{40}$$

This equation is also give the same equation as eq. 39.

For the sake of convenience, *partial cycle indices with chirality fittingness* for $\mathbf{G}_i$-symmetry are defined by the following equation:

$$\text{PCI-CF}(\mathbf{G}_i; \$_d) = \sum_{j=1}^{s} \overline{m}_{ij} \text{SCI-CF}(\mathbf{G}_j; \$_d) \quad (\text{for } i = 1, 2, \ldots, s), \tag{41}$$

where three types of sphericity indices are represented by $\$_d$ for the sake of simplicity. The following expression is formally obtained by combining eq. 40 with eq. 41 in order to memorize eq. 41:

$$(\ldots, \quad \text{PCI-CF}(\mathbf{G}_i; \$_d), \quad \ldots) = \left(\ldots, \quad \text{SCI-CF}(\mathbf{G}_j; \$_d), \quad \ldots\right) M_{\mathbf{G}}^{-1}. \tag{42}$$

Equation 41 is introduced into the right-hand side of eq. 39, giving the following theorem:

Theorem 4 (PCI Method). *Generating functions for calculating $B_{\theta i}$ ($i = 1, 2, \ldots, s$) are obtained as follows:*

$$\sum_{[\theta]} B_{\theta i} W_\theta = \text{PCI-CF}(\mathbf{G}_i; \$_d) \quad (\textit{for } i = 1, 2, \ldots, s), \tag{43}$$

where the sphericity indices (i.e., $\$_d = a_d, b_d$, or c_d) in the PCI-CF are substituted by the following ligand inventories:

$$a_d^{(\alpha)} = \mathrm{X}_1^d + \cdots + \mathrm{X}_x^d \tag{44}$$

$$c_d^{(\alpha)} = \mathrm{X}_1^d + \cdots + \mathrm{X}_x^d + 2(\mathrm{p}_1^{d/2}\overline{\mathrm{p}}_1^{d/2} + \cdots + \mathrm{p}_p^{d/2}\overline{\mathrm{p}}_p^{d/2}) \tag{45}$$

$$b_d^{(\alpha)} = (\mathrm{X}_1^d + \cdots + \mathrm{X}_x^d) + (\mathrm{p}_1^d + \cdots + \mathrm{p}_p^d) + (\overline{\mathrm{p}}_1^d + \cdots + \overline{\mathrm{p}}_p^d), \tag{46}$$

where the index α of each inventory corresponds to the USCI-CFs shown in the right-hand side of eq. 28 (via eq. 41).

This theorem is equivalent to Theorem 19.6 of Fujita's book [6]. The stereoisomer counting based on Theorem 4 is called *the PCI method*.[12]

The same results as shown in Table 3 are obtained as generating functions by means of the PCI method (Theorem 4). By following eq. 42, the USCI-CFs for the CR $\mathbf{D}_{2d}(/\mathbf{C}_s)$ (collected at the top of Table 1) are regarded as a row vector so as to give the following formal expression:

$$(b_1^4, b_2^2, b_2^2, a_1^2 c_2, c_4, a_2^2, b_4, a_4) M_{\mathbf{D}_{2d}}^{-1}. \tag{47}$$

Thereby, the following PCI-CFs are obtained by using the inverse mark table (eq. 17):

$$\text{PCI-CF}(\mathbf{C}_1; \$_d) = \frac{1}{8}b_1^4 - \frac{1}{8}b_2^2 - \frac{1}{4}b_2^2 - \frac{1}{4}a_1^2 c_2 + \frac{1}{4}a_2^2 + \frac{1}{4}b_4 \tag{48}$$

$$\text{PCI-CF}(\mathbf{C}_2; \$_d) = \frac{1}{4}b_2^2 - \frac{1}{4}c_4 - \frac{1}{4}a_2^2 - \frac{1}{4}b_4 + \frac{1}{2}a_4 \tag{49}$$

$$\text{PCI-CF}(\mathbf{C}_2'; \$_d) = \frac{1}{2}b_2^2 - \frac{1}{2}b_4 \tag{50}$$

$$\text{PCI-CF}(\mathbf{C}_s; \$_d) = \frac{1}{2}a_1^2 c_2 - \frac{1}{2}a_2^2 \tag{51}$$

$$\text{PCI-CF}(\mathbf{S}_4; \$_d) = \frac{1}{2}c_4 - \frac{1}{2}a_4 \tag{52}$$

$$\text{PCI-CF}(\mathbf{C}_{2v}; \$_d) = \frac{1}{2}a_2^2 - \frac{1}{2}a_4 \tag{53}$$

$$\text{PCI-CF}(\mathbf{D}_2; \$_d) = \frac{1}{2}b_4 - \frac{1}{2}a_4 \tag{54}$$

$$\text{PCI-CF}(\mathbf{D}_{2d}; \$_d) = a_4 \tag{55}$$

According to Theorem 4, the ligand inventories for this case are obtained as follows:

$$a_d = \mathrm{H}^d + \mathrm{X}^d \tag{56}$$

$$c_d = \mathrm{H}^d + \mathrm{X}^d + 2\mathrm{p}^{d/2}\overline{\mathrm{p}}^{d/2} \tag{57}$$

$$b_d = \mathrm{H}^d + \mathrm{X}^d + \mathrm{p}^d + \overline{\mathrm{p}}^d \tag{58}$$

[12] It should be noted that Theorem 4 involves Theorem 2.5 reported by Kerber [12] as a special case, because the latter theorem can be derived by the replacement of the USCI-CFs (or SCI-CFs) for Theorem 4 by the corresponding USCIs (or SCIs), where the three kinds of sphericity indices (a_d, b_d, and c_d) are replaced by a single dummy variable s_d. In other words, Theorem 4 takes account of the sphericities of the relevant orbits, whereas Theorem 2.5 (Kerber) lacks the concept of sphericity. This means that Theorem 2.5 (Kerber) is incapable of counting stereoisomers.

These inventories (eqs. 56–58) are introduced into the PCI-CFs (eqs. 48–55) to give the following generating functions:

$$\begin{aligned} f_{\mathbf{C}_1} &= \frac{1}{2}(\mathrm{H}^3\mathrm{p}+\mathrm{H}^3\overline{\mathrm{p}})+\frac{1}{2}(\mathrm{X}^3\mathrm{p}+\mathrm{X}^3\overline{\mathrm{p}})+ \\ &\quad +3\times\frac{1}{2}(\mathrm{H}^2\mathrm{Xp}+\mathrm{H}^2\mathrm{X}\overline{\mathrm{p}})+3\times\frac{1}{2}(\mathrm{HX}^2\mathrm{p}+\mathrm{HX}^2\overline{\mathrm{p}})+3\times\frac{1}{2}(\mathrm{HXp}^2+\mathrm{HX}\overline{\mathrm{p}}^2) \\ &\quad +(\mathrm{H}^2\mathrm{p}\overline{\mathrm{p}}+\mathrm{X}^2\mathrm{p}\overline{\mathrm{p}})+2\mathrm{HXp}\overline{\mathrm{p}} \\ &\quad +3\times\frac{1}{2}(\mathrm{Hp}^2\overline{\mathrm{p}}+\mathrm{Hp}\overline{\mathrm{p}}^2)+3\times\frac{1}{2}(\mathrm{Xp}^2\overline{\mathrm{p}}+\mathrm{Xp}\overline{\mathrm{p}}^2) \\ &\quad +\frac{1}{2}(\mathrm{Hp}^3+\mathrm{H}\overline{\mathrm{p}}^3)+\frac{1}{2}(\mathrm{Xp}^3+\mathrm{X}\overline{\mathrm{p}}^3)+\frac{1}{2}(\mathrm{p}^3\overline{\mathrm{p}}+\mathrm{p}\overline{\mathrm{p}}^3) \end{aligned} \tag{59}$$

$$f_{\mathbf{C}_2} = \frac{1}{2}(\mathrm{H}^2\mathrm{p}^2+\mathrm{H}^2\overline{\mathrm{p}}^2)+\frac{1}{2}(\mathrm{X}^2\mathrm{p}^2+\mathrm{X}^2\overline{\mathrm{p}}^2) \tag{60}$$

$$f_{\mathbf{C}_2'} = 2\times\frac{1}{2}(\mathrm{H}^2\mathrm{p}^2+\mathrm{H}^2\overline{\mathrm{p}}^2)+2\times\frac{1}{2}(\mathrm{X}^2\mathrm{p}^2+\mathrm{X}^2\overline{\mathrm{p}}^2)+\mathrm{p}^2\overline{\mathrm{p}}^2 \tag{61}$$

$$f_{\mathbf{C}_s} = (\mathrm{H}^3\mathrm{X}+\mathrm{HX}^3)+(\mathrm{H}^2\mathrm{p}\overline{\mathrm{p}}+\mathrm{X}^2\mathrm{p}\overline{\mathrm{p}})+2\mathrm{HXp}\overline{\mathrm{p}} \tag{62}$$

$$f_{\mathbf{S}_4} = \mathrm{p}^2\overline{\mathrm{p}}^2 \tag{63}$$

$$f_{\mathbf{C}_{2v}} = \mathrm{H}^2\mathrm{X}^2 \tag{64}$$

$$f_{\mathbf{D}_2} = \frac{1}{2}(\mathrm{p}^4+\overline{\mathrm{p}}^4) \tag{65}$$

$$f_{\mathbf{D}_{2d}} = (\mathrm{H}^4+\mathrm{X}^4). \tag{66}$$

The coefficients of the terms appearing in each of these generating functions are equal to the values appearing in the corresponding column of Table 3.

Exercise 13. Solve the same problem as Exercise 12 by using the PCI method (Theorem 4).

3.3.4 Cycle-Index (CI) Method for Stereoisomer Counting

If the itemization of point-group symmetries is unnecessary, a more simple theorem can be derived from Theorem 4. Let the symbol B_θ represent the number of stereoisomers with a weight W_θ. Then we obtain:

$$B_\theta = \sum_{i=1}^{s} B_{\theta i} \tag{67}$$

A cycle index with chirality fittingness CI-CF($\$_d$) is defined as follows:

$$\text{CI-CF}(\$_d) = \sum_{i=1}^{s} \text{PCI-CF}(\mathbf{G}_i;\$_d) \tag{68}$$

The PCI-CFs (eq. 43) are summed up over $\mathbf{G}_i$ and transformed by using eqs. 67 and 68 to give the following equation:

$$\sum_{[\theta]} B_\theta W_\theta = \sum_{[\theta]}\sum_{i=1}^{s} B_{\theta i} W_\theta = \sum_{i=1}^{s}\sum_{[\theta]} B_{\theta i} W_\theta = \sum_{i=1}^{s} \text{PCI-CF}(\mathbf{G}_i;\$_d) = \text{CI-CF}(\$_d) \tag{69}$$

Hence, Theorem 4 is transformed into a simple theorem:

Theorem 5 (CI Method). *A generating function for calculating B_θ is obtained as follows:*

$$\sum_{[\theta]} B_\theta W_\theta = \text{CI-CF}(\$_d) \tag{70}$$

where the sphericity indices (i.e., $\$_d = a_d, b_d$, or c_d) in the CI-CF are substituted by the following ligand inventories:

$$a_d^{(\alpha)} = \mathrm{X}_1^d + \cdots + \mathrm{X}_x^d \tag{71}$$

$$c_d^{(\alpha)} = \mathrm{X}_1^d + \cdots + \mathrm{X}_x^d + 2(\mathrm{p}_1^{d/2}\overline{\mathrm{p}}_1^{d/2} + \cdots + \mathrm{p}_p^{d/2}\overline{\mathrm{p}}_p^{d/2}) \tag{72}$$

$$b_d^{(\alpha)} = (\mathrm{X}_1^d + \cdots + \mathrm{X}_x^d) + (\mathrm{p}_1^d + \cdots + \mathrm{p}_p^d) + (\overline{\mathrm{p}}_1^d + \cdots + \overline{\mathrm{p}}_p^d), \tag{73}$$

where the index α of each inventory corresponds to the USCI-CFs shown in the right-hand side of eq. 28 (via eqs. 41 and 68).

This theorem is equivalent to Theorem 19.5 of Fujita's book [6] by considering Definition 19.7.[13]

The introduction of eq. 41 into eq. 68 and the subsequent transformation give the following equation:

$$\begin{aligned} \text{CI-CF}(\$_d) &= \sum_{i=1}^{s} \text{PCI-CF}(\mathbf{G}_i;\$_d) = \sum_{i=1}^{s}\sum_{j=1}^{s} \overline{m}_{ij}\text{SCI-CF}(\mathbf{G}_j;\$_d) \\ &= \sum_{j=1}^{s} (\sum_{i=1}^{s} \overline{m}_{ij})\text{SCI-CF}(\mathbf{G}_j;\$_d), \end{aligned} \tag{74}$$

where the exchange of the order of the summations is permissible because the SCI-CF is common with respect to each $\mathbf{G}_j$-row of the inverse mark table ($M_{\mathbf{G}}^{-1}$). The summation ($\sum_{i=1}^{s} \overline{m}_{ij}$ for $j = 1, 2, \ldots, s$) represents a one-column matrix, each element of which are the sum of each row of the inverse mark table (for each $\mathbf{G}_j$).[14] For example, the right margin of the $M_{\mathbf{D}_{2d}}^{-1}$ (eq. 17) shows the sum of each row to exemplify eq. 74.

By following Theorem 5, eqs. 48–55 are summed up so as to give a CI-CF for this case:

$$\text{CI-CF}(\$_d) = \frac{1}{8}b_1^4 + \frac{1}{8}b_2^2 + \frac{1}{4}b_2^2 + \frac{1}{4}a_1^2c_2 + \frac{1}{4}c_4 \tag{75}$$

The same CI-CF can be obtained by using the summed matrix shown in the right margin of the $M_{\mathbf{D}_{2d}}^{-1}$ (eq. 17) according to eq. 74. By introducing the ligand inventories shown in eqs. 56–58, eq. 75 is transformed into a generating function for this case:

$$f_{\text{total}} = (\mathrm{H}^4 + \mathrm{X}^4) + (\mathrm{H}^3\mathrm{X} + \mathrm{H}\mathrm{X}^3) + 2\mathrm{H}^2\mathrm{X}^2$$

[13] It should be noted that Theorem 5 involves Pólya's theorem [2, 3] as a special case, because the latter theorem can be derived by the replacement of the USCI-CFs (or SCIs) for Theorem 5 by the corresponding USCIs (or SCIs), where the three kinds of sphericity indices (a_d, b_d, and c_d) are replaced by a single dummy variable s_d. In other words, Theorem 5 takes account of the sphericities of the relevant orbits, whereas Pólya's theorem lacks the concept of sphericity. This means that Pólya's theorem is incapable of counting stereoisomers. This point has been discussed in recent papers [4, 5].

[14] The properties of the summation have been discussed in Section 16.2 of Fujita's book [6]. Thus, the sum for each cyclic subgroup has a non-zero value, while the sum for each non-cyclic subgroup is equal to zero.

$$
\begin{aligned}
&+\frac{1}{2}(\mathrm{H}^3\mathrm{p}+\mathrm{H}^3\overline{\mathrm{p}})+\frac{1}{2}(\mathrm{X}^3\mathrm{p}+\mathrm{X}^3\overline{\mathrm{p}})\\
&+3\times\frac{1}{2}(\mathrm{H}^2\mathrm{X}\mathrm{p}+\mathrm{H}^2\mathrm{X}\overline{\mathrm{p}})+3\times\frac{1}{2}(\mathrm{H}\mathrm{X}^2\mathrm{p}+\mathrm{H}\mathrm{X}^2\overline{\mathrm{p}})\\
&+3\times\frac{1}{2}(\mathrm{H}^2\mathrm{p}^2+\mathrm{H}^2\overline{\mathrm{p}}^2)+3\times\frac{1}{2}(\mathrm{X}^2\mathrm{p}^2+\mathrm{X}^2\overline{\mathrm{p}}^2)+3\times\frac{1}{2}(\mathrm{H}\mathrm{X}\mathrm{p}^2+\mathrm{H}\mathrm{X}\overline{\mathrm{p}}^2)\\
&+(2\mathrm{H}^2\mathrm{p}\overline{\mathrm{p}}+2\mathrm{X}^2\mathrm{p}\overline{\mathrm{p}})+4\mathrm{H}\mathrm{X}\mathrm{p}\overline{\mathrm{p}}\\
&+3\times\frac{1}{2}(\mathrm{H}\mathrm{p}^2\overline{\mathrm{p}}+\mathrm{H}\mathrm{p}\overline{\mathrm{p}}^2)+3\times\frac{1}{2}(\mathrm{X}\mathrm{p}^2\overline{\mathrm{p}}+\mathrm{X}\mathrm{p}\overline{\mathrm{p}}^2)\\
&+\frac{1}{2}(\mathrm{H}\mathrm{p}^3+\mathrm{H}\overline{\mathrm{p}}^3)+\frac{1}{2}(\mathrm{X}\mathrm{p}^3+\mathrm{X}\overline{\mathrm{p}}^3)\\
&+2\mathrm{p}^2\overline{\mathrm{p}}^2+\frac{1}{2}(\mathrm{p}^3\overline{\mathrm{p}}+\mathrm{p}\overline{\mathrm{p}}^3)+\frac{1}{2}(\mathrm{p}^4+\overline{\mathrm{p}}^4) \qquad (76)
\end{aligned}
$$

The coefficient of each term (or each combined term) represents the total number of stereoisomers with the corresponding weight (molecular formula), where the total number is equal to the summed value collected in the right-most column of Table 3.

Exercise 14. Place $s_d = a_d = b_d = c_d$ in eq. 75. Show that the resulting cycle index (CI) is equivalent to the one obtained by Pólya's theorem. Examine the effect of the sphericity concept by comparing between the CI-CF (i.e., cycle index with chirality fittingness) the CI (i.e., cycle index without chirality fittingness). Then, introduce the ligand inventory $s_d = \mathrm{H}^d + \mathrm{X}^d$ into the CI. See Chapter 13 of Fujita's book [6].

Exercise 15. Solve the problem described in Exercise 12 (or 13) by using the CI method (Theorem 5).

4 Perspectives

It is worthwhile to mention supplementary comments on Fujita's USCI approach, which would provide us with further perspectives on stereochemistry and chemical combinatorics.

1. As an alternative methodology other than generating functions, the concept of *elementary superposition* has been proposed by Fujita in order to take account of sphericities in combinatorial enumeration considering weights and point-group symmetries [13].[15] Thus, two methods based on the elementary superposition have been developed and compared with the two methods based on generating functions (the SCI method and the PCI method) [14]. The concept of elementary superposition should be studied by means of the diagrammatical approach described in Parts 1–3.

2. As an alternative method other than the CI method, the characteristic-monomial (CM) method should be introduced here, because the CM method is based on linear representations and Q-conjugacy characters [15, 16, 17]. The CM method has been compared with the USCI approach which is based on permutation representations (coset representations) and marks [18]. Although the CM method has less advantage than Theorem 5 of the USCI approach, the comparison between them has provided us with an insight to comprehend group theoretical concepts such as linear representations and permutation representations. A diagrammatical explanation of the CM method remains unsolved.

[15] A version without taking account of sphericities has been described in Chapter 18 of Fujita's book [6].

3. Theorem 5 is superior over Pólya's theorem in the capability of enumerating stereoisomers. Because Theorem 5 is based on conjugate subgroups via marks, a more straightforward theorem based on conjugacy classes is desirable. Although this has been reported by Fujita [4, 5], further extensions and diagrammatical explanations are necessary.

4. The concepts of mandalas and reduced mandalas have brought about new structures, which should be studied group-theoretically in terms of viewpoints other than the present diagrammatical approach.

5. The USCI approach is capable of comprehending the relationships between graphs and 3D structures, because USCI-CFs for 3D structures are easily replaced by USCIs to discuss graphs. Reversely, a general method for converting graphs into 3D structures requires further studies.

6. In Part 2 and Part 3, enantiomers have been successfully treated by the concept of sphericity, which is based on the combination of point-group theory and permutation-group theory. In other words, enantiomers can be formulated as equivalence classes in terms of the combination. However, diastereomers have been characterized implicitly by the difference in molecular formulas. The explicit characterization of diastereomers as equivalence classes has been reported to require more extended groups, e.g., *RS*-stereoisomeric groups [19, 20, 21]. Although an intuitive explanation based on stereoisograms has been reported [22], more diagrammatical explanations for these groups are necessary.

5 Conclusions

The four positions of an allene skeleton construct an orbit governed by the CR $\mathbf{D}_{2d}(/\mathbf{C}_s)$, where the subduction $\mathbf{D}_{2d}(/\mathbf{C}_s) \downarrow \mathbf{H}$ generates the unit subduced cycle index with chirality fittingness (USCI-CF) of the subgroup **H** (Part 1 of this series). The USCI-CF is used to generate a generating function for evaluating the number of fixed points for each subgroup **H**, where the number is regarded as the **H**-element in the fixed point vector (FPV) of molecules of **H** or its supergroup symmetries. The FPV evaluation is formulated in terms of the "column view" of the mark table of $\mathbf{D}_{2d}$.

On the other hand, each row of the mark table of $\mathbf{D}_{2d}$ is recognized as an FPV of the corresponding CR $\mathbf{D}_2(/\mathbf{H})$ which governs an orbit of **H**-assemblies in a reduced mandala of $\mathbf{D}_{2d}$ (Part 2 of this series). The FPV recognition is formulated in terms of the "row view" of the mark table of $\mathbf{D}_{2d}$.

Because each of the **H**-assemblies represents a molecule of **H**-symmetry, the FPV of the row views can be correlated to the FPV of the column view. The integration of the two modes of views provides us with a versatile tool for enumerating stereoisomers, i.e., the subduced-cycle-index (SCI) method. Thereby, the fixed-point-matrix (FPM) that consists of such FPVs as calculated by the SCIs is multiplied by the inverse of the mark table. Thereby, an isomer-counting matrix (ICM) is obtained to show stereoisomer numbers that are itemized with respect to molecular formulas and point group symmetries.

By starting from the SCI method, another tool (the partial-cycle-index (PCI) method) is developed to derive generating functions for enumerating stereoisomers with respect to molecular formulas and point group symmetries.

References

[1] Balaban, A. T. eds. (1976) *Chemical Applications of Graph Theory* (Academic Press, London).

[2] Pólya, G. (1937) *Acta Math.* **68**, 145–254.

[3] Pólya, G. & Read, R. C. (1987) *Combinatorial Enumeration of Groups, Graphs, and Chemical Compounds* (Springer-Verlag, New York).

[4] Fujita, S. (2005) *Theor. Chem. Acc.* **113**, 73–79.

[5] Fujita, S. (2005) *Theor. Chem. Acc.* **113**, 80–86.

[6] Fujita, S. (1991) *Symmetry and Combinatorial Enumeration in Chemistry* (Springer-Verlag, Berlin-Heidelberg).

[7] Fujita, S. (2005) *MATCH Commun. Math. Comput. Chem.* **54**, 251–300.

[8] Fujita, S. (2006) *MATCH Commun. Math. Comput. Chem.* **55**, 5–38.

[9] Burnside, W. (1911) *Theory of Groups of Finite Order* 2nd edn. (Cambridge University Press, Cambridge).

[10] Fujita, S. (1990) *J. Math. Chem.* **5**, 121–156.

[11] Fujita, S. (1989) *Theor. Chim. Acta* **76**, 247–268.

[12] Kerber, A. & Thürlings, K.-J. (1982) in *Combinatorial Theory*, ed. Jngnickel, D. & Vedder, K. (Springer, Berlin), pp. 191–211.

[13] Fujita, S. (1992) *Theor. Chim. Acta* **82**, 473–498.

[14] Fujita, S. (1993) *J. Math. Chem.* **12**, 173–195.

[15] Fujita, S. (1998) *Theor. Chem. Acc.* **99**, 224–230.

[16] Fujita, S. (1998) *Theor. Chem. Acc.* **99**, 404–410.

[17] Fujita, S. (1999) *Theor. Chem. Acc.* **101**, 409–420.

[18] Fujita, S. (2001) *J. Math. Chem.* **30**, 249–270.

[19] Fujita, S. (2004) *MATCH Commun. Math. Comput. Chem.* **52**, 3–18.

[20] Fujita, S. (2004) *J. Chem. Inf. Comput. Sci.* **44**, 1719–1726.

[21] Fujita, S. (2005) *MATCH Commun. Math. Comput. Chem.* **53**, 147–159.

[22] Fujita, S. (2004) *J. Org. Chem.* **69**, 3158–3165.